Assessment of design models for aluminium alloy CHS beam-columns with stocky cross-sections

Authors:

Michaela Gkantou[a], Nikolaos I. Tziavos[b], Samir Dirar[c,d], Marios Theofanous[d], Oghenelukume Pearl Ukpedor[e], Andrew Foster[f]

[a]School of Civil Engineering and Built Environment, Liverpool John Moores University, UK

[b]Department of Civil Engineering, Aston University, UK

[c]University of Sharjah, College of Engineering, Department of Architectural Engineering, UAE (email: sdirar@sharjah.ac.ae)

[d]Department of Civil Engineering, University of Birmingham, UK

[e]Meinhardt Ltd, UK

[f]HSP consulting, Birmingham, UK

ABSTRACT

There is little information on the prediction accuracy of the international design standards for aluminium alloy circular hollow section (CHS) beam-columns. To bridge this gap, this paper presents a comprehensive numerical investigation on the performance of aluminium alloy CHS beam-columns with stocky cross-sections. A non-linear finite element (FE) model was developed and validated against experimental results. The validated FE model was employed to conduct an extensive parametric study of aluminium CHS members subjected to combined axial compression and bending over a range of lengths, cross-sections and applied eccentricities. The effect of these parameters was investigated for two material grades, 6061-T6 and 6082-T6, resulting in a total of 168 FE models. The numerically obtained capacities were used to assess the accuracy of the strength predictions of Eurocode 9 (EC9), the Aluminium Design Manual (AA) and the Direct Strength Method (DSM). On the basis of the results, EC9, with the exponent of the interaction formula, ψ_c, calculated as a function of the buckling reduction factor χ, was found to provide the most accurate strength predictions with a mean value equal to 1.01 for both examined material grades. The most conservative predictions were given by the DSM, whilst the most scattered predictions by the AA, with a Coefficient of Variation (COV) equal to 0.17. Finally, based on the DSM buckling strength

and the plastic cross-sectional moment resistance, a new interaction curve is proposed for CHS beam-columns with stocky cross-sections.

Keywords: Aluminium Alloy; Circular Hollow Sections; Beam-columns; Eurocodes; Direct Strength Method; Aluminum Association

1. Introduction

Hollow aluminium structural members are extensively utilised within the aerospace and automotive sectors, owing to the combined high strength-to weight ratio and flexibility. On the contrary, the adoption of aluminium in the construction industry is still limited. Due to aluminium's Young's Modulus being roughly one-third that of steel, the design of structural members poses a challenge, as they are prone to instability induced failure modes and excessive deflections.

In recent years, there has been a significant increase in research studies investigating different cross-sections and members made from structural aluminium alloys (Georgantzia et al., 2021a). Even though considerable emphasis has been placed on square and rectangular hollow sections (SHS, RHS) (e.g. Su et al., 2016; Wang et al., 2016; Castaldo et al., 2017; Feng et al., 2019; Georgantzia et al., 2021b; Bock et al., 2021; Hu et al., 2021; Li et al., 2022a; Li et al., 2022b; Li et al., 2022d; Rong et al., 2022a; Ali et al., 2022; Zhi et al., 2022; Nastri et al., 2022), studies on the performance of aluminium alloy circular hollow sections (CHS) remain relatively limited. In particular, the performance of circular hollow sections was studied by Wang et al. (2015, 2016) who examined experimentally and numerically the performance of aluminium alloy 6082 circular tubes in axial compression. Feng et al. (2016, 2020) focused on perforated CHS aluminium beams and columns. Zhu and Young (2008) examined the performance of CHS columns, whilst recently Li et al. (2022c) investigated the ultimate response of CHS 7A04-T6 columns. All these studies focus either on axial compression or pure bending performance without any consideration of the combined compression and bending response.

Aluminium circular hollow sections are highly vulnerable to buckling failures when subjected to a combination of axial compression and bending, therefore their response under this loading regime requires careful consideration. The authors have identified only a few studies on CHS aluminium beam-columns, namely a relatively old, experimental study by Zhu and Young (2006), who tested 6082-T6 CHS members subjected to various eccentric compressive loads, concluding that the European (EC9, 2000), American (Aluminium design manual, 2000) and Australian/New Zealand (AS/NZS, 1997) design models used for predicting the capacity of beam-column members produce conservative results. Zhao and Zhai (2019a, 2019b) investigated the performance of SHS and CHS aluminium alloy beam-columns and proposed a modification for the Chinese design code. More recently, Rong *et al.* (2022b)

examined the performance of 7A04-T6 CHS members under eccentric compression and assessed the European design guidelines, concluding conservative design predictions. Considering the above, it is deemed necessary to assess the accuracy of some of the internationally used design models for CHS aluminium alloy beam-columns in order to prevent inefficient design. Herein focus is placed on CHS beam-columns with stocky cross-sections in Grades 6082-T6 and 6061-T6 material grades, given that these grades are among the most widely used in construction. The results of a series of experimental studies on aluminium alloy CHS members are selected (Section 2) and utilised for the validation of an FE model. The nonlinear FE model is presented in Section 3 and the validation study in Section 4. In Section 5, a comprehensive parametric study on members with stocky cross-sections is presented, investigating beam-columns with different lengths, cross-sectional geometries, and material properties. The numerically obtained strengths are compared with predicted design capacities in Section 6 to evaluate the codified design provisions of EN 1999-1-1 (2007), the Direct Strength Method (Schafer, 2008) and Aluminium Design Manual (AA, 2015). Finally, the main conclusions of this study are presented in Section 7.

2. Experimental database

Experimental and numerical data on aluminium CHS beam-columns are scarce. Nevertheless, it is critical to ensure that the numerical model is able to accurately capture the response of two direct loading conditions – axial compression and pure bending, as well as eccentric loading. For this purpose, the model was validated against four published datasets published in the literature (Wang et al., 2015; Zhu and Young, 2006; Feng et al., 2020, Zhao and Zhai, 2020). A total of 34 experiments were employed, comprising 8 columns, 20 beams and 6 beam-columns, as shown in Table 1, where the specimens' notation is the same as in the relevant publications. In Figure 1, the experimental set-up which was used in the respective paper is shown. The main set-up components together with the applied instrumentation during loading is also shown in this figure. Key test values, such as the main cross-sectional properties (diameter D, thickness t), the specimen's length (L), the eccentricity of the applied load (not relevant for the beams), the ultimate load ($N_{u,Exp}$) and moment ($M_{u,Exp}$) values, as achieved during the tests, are listed for reference in Table 2. The selected experimental studies comprised circular hollow sections made from 6082-T6 and 6061-T6, whose Young's Modulus (E), proof strength ($\sigma_{0.2}$), strain hardening component (n) and ultimate strength (σ_u) are also listed in the

same table. These two grades, which are commonly used in structural engineering, will also be the focus in the numerical study.

Table 1: Tests used for validation purposes.

Reference	Type	Specimen name (based on references)	Material
Wang et al. (2015)	Columns (8 tests)	O89-L500-A O89-L800-A O89-L800-C O89-L1200-B O89-L1650-A O89-L1650-B O89-L1650-C O76-L1700-A	6082-T6
Zhu and Young (2006)	Beams (20 tests)	C1 BEAM C2 BEAM	6061-T6
Feng et al. (2020)		HC150x7-B4	6061-T6
Zhao and Zhi (2020)		CHS-89-4-1800A CHS-89-4-1800B CHS-89-4-1800C CHS-89-4-2200A CHS-89-5-1800A CHS-89-5-1800B CHS-89-5-2200A CHS-89-5-2200B CHS-114-4-1800A CHS-114-4-2200A CHS-114-4-2200B HS-114-5.5-1800A CHS-114-5.5-2200A CHS-114-7-1800A CHS-114-7-1800B CHS-114-7-2200A CHS-114-7-2200B	6082-T6
Zhu and Young (2006)	Beam-columns (6 tests)	C1L500E15 C1L500E40 C1L1000E15 C1L1000E45 C2L1000E15 C2L1000E50	6061-T6

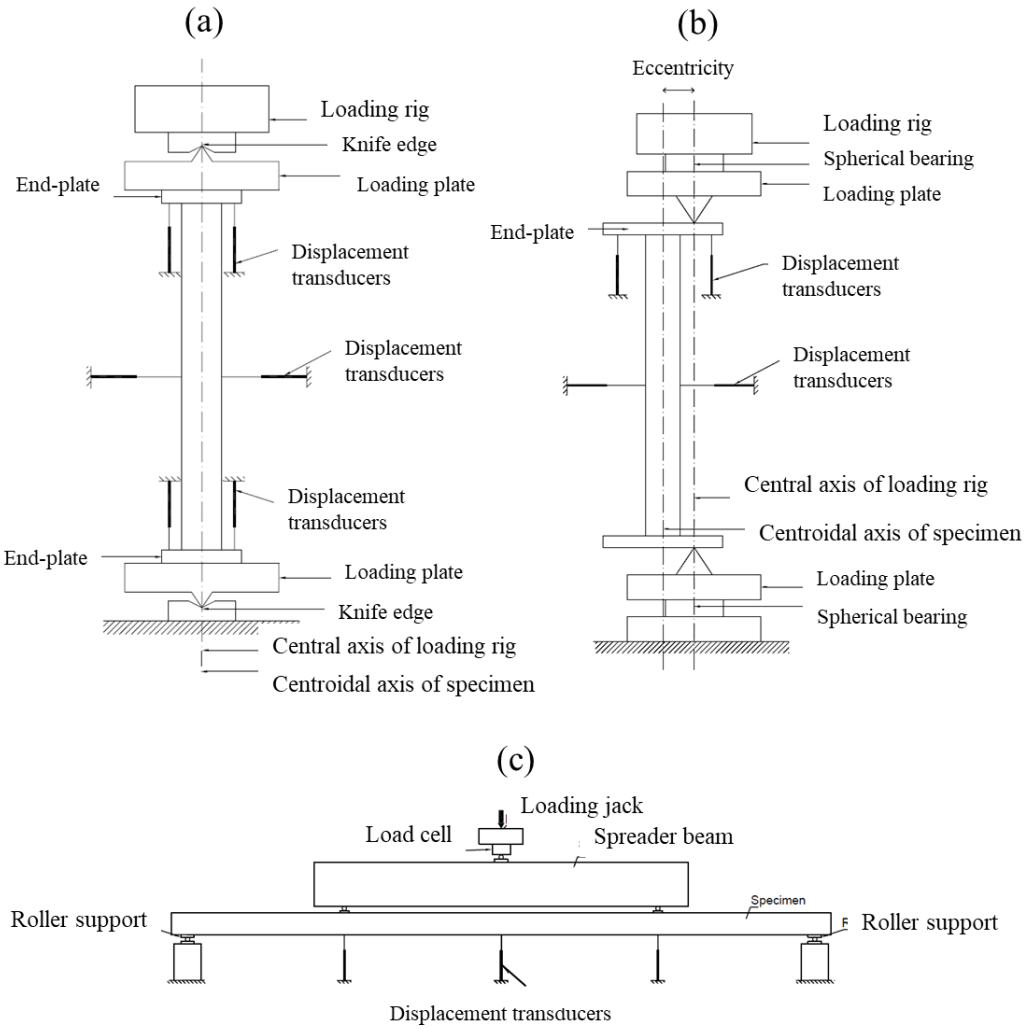

106

107 Figure 1: Experimental set-ups. a) column experiment, adapted from Wang et al., 2015, b)
108 beam-column experiment, adapted from Zhu and Young, 2006, c) beam experiment, adapted
109 from Feng et al., 2020, Zhao and Zhai, 2020.

110

Table 2: Summary of experimental results.

Reference	Specimen name	D (mm)	t (mm)	L (mm)	e (mm)	E (MPa)	$\sigma_{0.2}$ (MPa)	σ_u (MPa)	$N_{u,Exp}$ (kN)	$M_{u,Exp}$ (kNm)
Wang et al. (2015)	O89-L500-A	88.80	6.29	500.5	0.693	70233	272.22	(n=25.24)	508.71	-
	O89-L800-A	88.80	6.29	800.0	1.160	70233	272.22	(n=25.24)	444.26	-
	O89-L800-C	88.81	6.29	799.0	0.349	70233	272.22	(n=25.24)	473.67	-
	O89-L1200-B	88.81	6.29	1200.0	1.049	70233	272.22	(n=25.24)	378.68	-
	O89-L1650-A	88.62	6.31	1649.0	6.361	70233	272.22	(n=25.24)	239.67	-
	O89-L1650-B	88.63	6.30	1650.0	1.184	70233	272.22	(n=25.24)	269.84	-
	O89-L1650-C	88.70	6.29	1650.0	1.997	70233	272.22	(n=25.24)	265.55	-
	O76-L1700-A	75.51	2.81	1700.0	2.239	70233	272.22	(n=25.24)	74.17	-
Zhu and Young (2006)	C1 BEAM	49.80	1.59	1000.0	-	67100	286.70	310.10	-	1.15
	C2 BEAM	49.80	3.08	1000.0	-	73400	242.80	262.80	-	2.14
Feng et al. (2020)	HC150x7-B4	202.53	7.57	2699.9	-	69700	198.72	218.64	-	65.60
Zhao and Zhai (2020)	CHS-89-4-1800A	88.62	3.80	1800	-	68190	285.00	(n=28.5)	-	8.24
	CHS-89-4-1800B	88.63	3.88	1800	-	68190	285.00	(n=28.5)	-	8.06
	CHS-89-4-1800C	88.83	3.90	1800	-	68190	285.00	(n=28.5)	-	8.47
	CHS-89-4-2200A	88.41	3.92	2200	-	68190	285.00	(n=28.5)	-	7.66
	CHS-89-5-1800A	88.89	4.97	1800	-	68190	285.00	(n=28.5)	-	11.21
	CHS-89-5-1800B	89.12	5.08	1800	-	68190	285.00	(n=28.5)	-	10.67
	CHS-89-5-2200A	88.82	4.99	2200	-	68190	285.00	(n=28.5)	-	10.63
	CHS-89-5-2200B	88.94	4.99	2200	-	68190	285.00	(n=28.5)	-	11.09
	CHS-114-4-1800A	114.22	3.93	1800	-	68190	285.00	(n=28.5)	-	16.00
	CHS-114-4-2200A	114.42	4.03	2200	-	68190	285.00	(n=28.5)	-	14.17
	CHS-114-4-2200B	113.96	4.06	2200	-	68190	285.00	(n=28.5)	-	14.50
	CHS-114-5.5-1800A	113.84	5.55	1800	-	68190	285.00	(n=28.5)	-	18.93
	CHS-114-5.5-2200A	114.16	5.45	2200	-	68190	285.00	(n=28.5)	-	19.24
	CHS-114-7-1800A	113.99	6.90	1800	-	68190	285.00	(n=28.5)	-	25.61
	CHS-114-7-1800B	113.46	6.76	1800	-	68190	285.00	(n=28.5)	-	24.81
	CHS-114-7-2200A	113.61	6.90	2200	-	68190	285.00	(n=28.5)	-	26.03
	CHS-114-7-2200B	113.84	6.90	2200	-	68190	285.00	(n=28.5)	-	24.83
	CHS-89-4-1800A	88.62	3.80	1800	-	68190	285.00	(n=28.5)	-	8.240
Zhu and Young (2006)	C1L500E15	50.00	1.57	500.1	14.6	67100	286.70	310.10	29.1	0.569
	C1L500E40	50.10	1.56	500.0	42.7	67100	286.70	310.10	16.8	0.894
	C1L1000E15	50.00	1.55	1000.4	17.8	67100	286.70	310.10	19.9	0.912
	C1L1000E45	50.10	1.55	1000.0	46.9	67100	286.70	310.10	12.0	0.931
	C2L1000E15	49.70	3.05	1000.0	16.0	67100	286.70	310.10	36.0	1.469
	C2L1000E50	49.80	3.04	1000.0	50.5	67100	286.70	310.10	20.0	1.727

3. Numerical Modelling Assumptions

The finite element models of the aluminium alloy CHS specimens were developed using the commercial software package Abaqus (2021). Initially, the midline dimensions of the cross-section were modelled, in line with previously published studies on thin-walled metallic sections (Wang et al, 2016; Gkantou et al., 2017a). Four node double-curved shell elements with reduced integration were employed to avoid shear and membrane locking of models. Subsequently, the specimens were extruded to their desired lengths, as shown in Figure 2. The

material response which indicated rounded response (was approximated based on Ramberg and Osgood (1943) model and was modelled with the Von Mises yield criterion with isotropic hardening, using the elastic and plastic material properties reported in the respective experimental studies.

The adopted boundary conditions aimed to simulate those presented in Figure 1, for each test type. For the column and the beam-column members, the top of the specimens can rotate and longitudinally shorten, whereas the bottom is modelled as pinned. By assigning the boundary conditions and tying the cross-section end nodes to a reference point (RP-TOP, RP-BOTTOM), the rotational point of both knife edges in the experimental testing can be modelled, ensuring the numerical analysis can capture an accurate response of the deformations. The load is then applied to the top reference point, as shown in Figure 2. Contrary to the columns, where the axial compressive load is applied concentrically, in the beam-column models, the compressive load is applied with an eccentricity from the cross-sectional centroid, as reported in Table 2.

The development of the FE models for the four-point bending tests was similar to that of the column and beam-column members in terms of chosen element type and material model. Simply supported beam boundary conditions restricted displacement in the x and y-axis (U1 and U2) at the support location (see Figure 2(c)). Following the reported testing procedures, steel stiffeners were used to reinforce the areas susceptible to local bearing failure located at the support and loading points and were included in the numerical analysis by utilising kinematic coupling constraints. This ensured the cross-section was rigid at the support and loading locations, whilst applying the assigned boundary conditions across the whole cross-section. According to the reported experimental studies, the beam was subjected to pure bending in the central moment region.

Initial geometric imperfections can affect the buckling response of thin-walled metallic structures. A linear perturbation buckling analysis is initially used to extract the eigenvalues. The lowest local and global buckling mode shapes are imported as initial geometric imperfections in the subsequent nonlinear analysis, which is executed with the general static Riks method. The amplitude of the required initial geometric imperfection size to accurately simulate the members considered is determined based on a sensitivity analysis reported in the next section.

- Rigid body at RP-TOP
- BC at RP-TOP:

$u_x=u_y=u_{rz}=0$, $u_z\neq0$, $u_{rx}\neq0$, $u_{ry}\neq0$

- Downwards vertical load at RP-TOP

- Rigid body at RP-BOTTOM
- BC at RP-BOTTOM:

$u_x=u_y=u_z=u_{rz}=0$, $u_{rx}\neq0$, $u_{ry}\neq0$

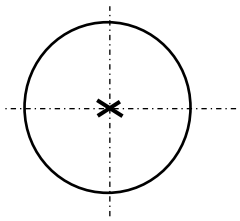

RP-TOP
RP-BOTTOM
} At centroid

(a) columns

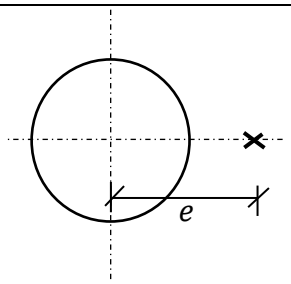

RP-TOP
RP-BOTTOM
} At distance *e* (eccentricity) from centroid

(b) beam-columns

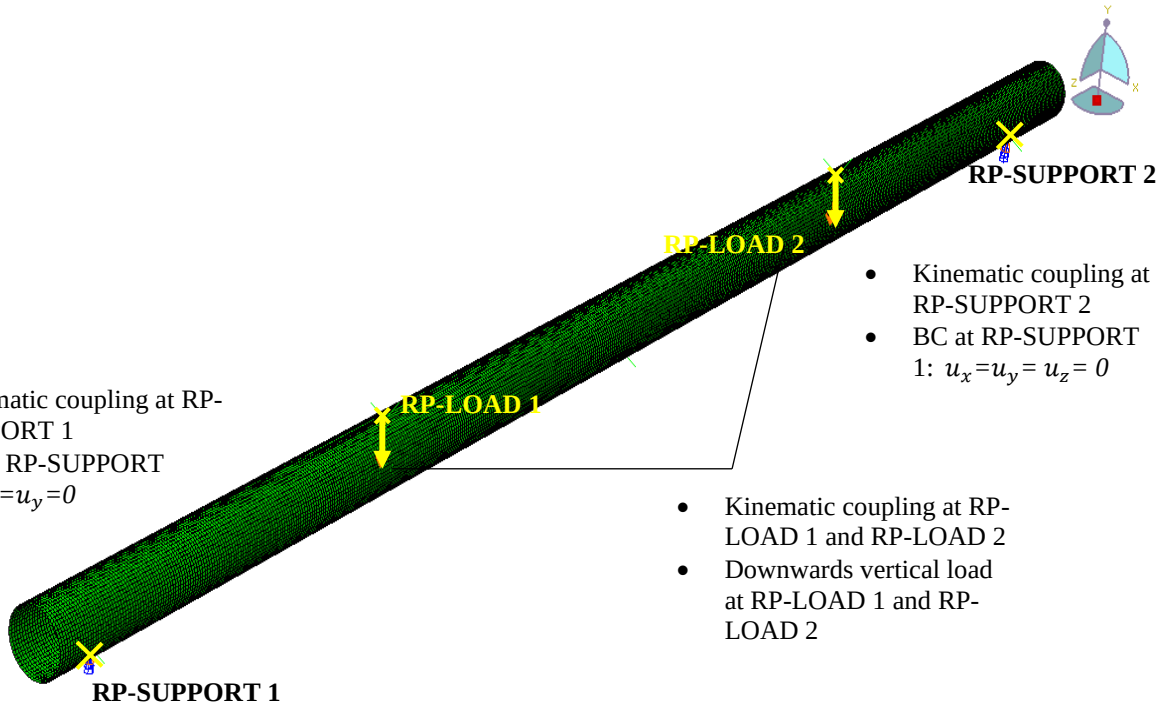

- Kinematic coupling at RP-SUPPORT 2
- BC at RP-SUPPORT 1: $u_x=u_y=u_z=0$

- Kinematic coupling at RP-SUPPORT 1
- BC at RP-SUPPORT 1: $u_x=u_y=0$

- Kinematic coupling at RP-LOAD 1 and RP-LOAD 2
- Downwards vertical load at RP-LOAD 1 and RP-LOAD 2

(c) beams

Figure 2: Numerical Models.

To optimise the computational time required for the simulations whilst ensuring the results of the analysis are not affected by mesh size, a mesh convergence study was also performed on the models. Six different mesh configurations, with average element size given as a function of the cross-section's diameter (D/6, D/8, D/10, D/15, D/20, D/25), were examined and the elastic critical buckling stress, σ_{cr}, was calculated. Once the difference between two consecutive mesh sizes was below 1%, it was concluded that a further decrease of the mesh size would not contribute to increased accuracy. Typical examples from the mesh convergence study for a numerically modelled column, beam-column and beam are shown in Figure 3. Overall, it was found that D/20 was the optimum mesh size and therefore it was used for further analysis in Sections 4 and 5.

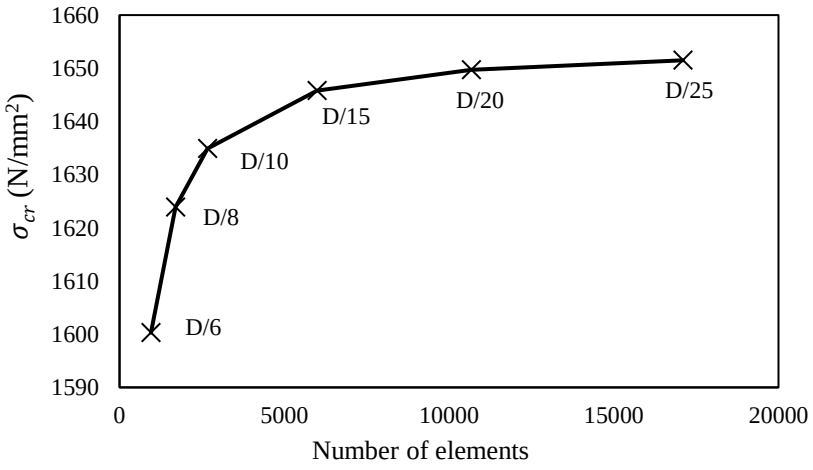

(a) columns (O89-L800-A)

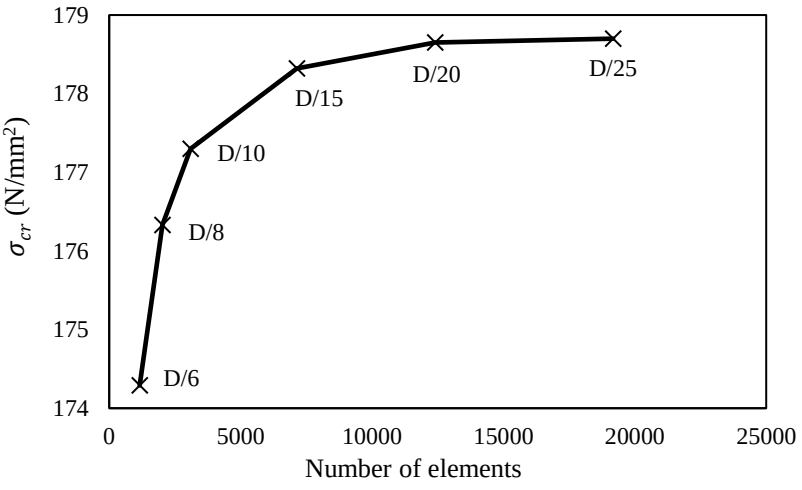

(b) beam-columns (C1L500E15)

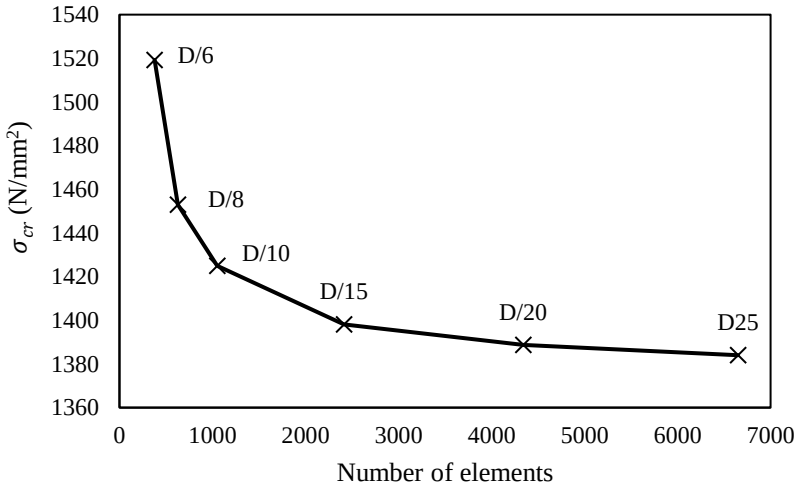

(c) beams (HC150x7-B4)

Figure 3: Mesh study - typical cases for each studied member.

Finally, the residual stresses have been found to have little influence on the load-carrying capacities of extruded aluminium alloy profiles (Mazzolani, 1995). In line with past studies (Feng et al., 2019; Georgantzia et al., 2023), they were not explicitly included in the FE models developed herein. Nevertheless, very good agreement between experimental and numerical performance has been achieved, as will be shown in the following section.

4. Validation of the FE models

The numerical models were validated by comparing the experimentally obtained ultimate loads and moments against the corresponding numerical values (Table 3), the overall load-deflection curves (Figure 4) and failure modes (Figure 5). A geometric imperfection sensitivity study was initially performed on the FE models to help identify which local and global geometric imperfection amplitudes obtained the best agreement between the experimental data and numerical results. Four different combinations of imperfection amplitudes were used in the imperfection study, for the columns and beam-columns, considering imperfection amplitudes as fractions of the section thickness and member length for buckling mode shapes pertinent to local and global buckling respectively: t/10 + L/1000, t/10 + L /1500, t/100+ L/1000, t/100 + L /1500. For the beam models, two local geometric imperfection amplitudes were examined: t/10, and t/100. The comparison of the experimental-to-numerical capacity values are shown in Table 3. When comparing the ultimate axial load ratios ($N_{u,Exp}/N_{u,FE}$) for the columns and beam-columns specimens, it was found that the imperfection amplitude t/10 + L/1000 led to the best agreement between the experimental and numerical ultimate capacities, achieving a

mean ratio of 0.98 and 0.96, respectively. Whilst the local geometric amplitude of *t*/10 did not lead to the best agreement between the experimental beam results and the corresponding FE predictions, overall it provided a successful validation and hence it was deemed accurate enough and will be used in the subsequent parametric study. In Figure 4, typical load-deflection curves are presented, showing a successful replication of the experimental response by the numerical models. Finally, successfully validated failure modes are depicted in Figure 5.

Table 3: Comparison of experimental and numerical ultimate response including an imperfection sensitivity study.

(a) columns

	Imperfection Magnitude			
	t/10 + L/1000	t/10 + L/1500	t/100 + L/1000	t/100 + L/1500
Specimen	$N_{u,Exp}/N_{u,FE}$	$N_{u,Exp}/N_{u,FE}$	$N_{u,Exp}/N_{u,FE}$	$N_{u,Exp}/N_{u,FE}$
C1L500E15	0.99	0.99	0.97	0.97
C1L500E40	0.98	0.98	0.95	0.95
C1L1000E15	1.00	1.00	1.00	1.00
C1L1000E45	0.96	0.96	0.96	0.96
C2L1000E15	1.00	1.00	0.99	0.99
C2L1000E50	0.96	0.96	0.96	0.96
Mean	0.98	0.98	0.97	0.97
COV	0.02	0.02	0.02	0.02

(b) beam-columns

	Imperfection Magnitude			
	t/10 + L/1000	t/10 + L/1500	t/100 + L/1000	t/100 + L/1500
Specimen	$N_{u,Exp}/N_{u,FE}$	$N_{u,Exp}/N_{u,FE}$	$N_{u,Exp}/N_{u,FE}$	$N_{u,Exp}/N_{u,FE}$
O89-L500-A	1.01	1.01	0.99	0.99
O89-L800-A	0.97	0.96	0.96	0.96
O89-L800-C	1.01	1.00	1.01	1.00
O89-L1200-B	1.11	1.09	1.11	1.09
O89-L1650-A	0.82	0.81	0.81	0.80
O89-L1650-B	0.94	0.91	0.94	0.91
O89-L1650-C	0.95	0.93	0.95	0.93
O77-L1700-A	0.85	0.82	0.85	0.81
Mean	0.96	0.94	0.95	0.94
COV	0.10	0.10	0.10	0.10

(c) beams

	Imperfection Magnitude	
Specimen	t/10	t/100
	$M_{u,Exp}$ / $M_{u,FE}$	$M_{u,Exp}$ / $M_{u,FE}$

C1 BEAM	1.14	1.11
C2 BEAM	1.07	1.04
HC150x7-B4	1.01	0.99
CHS-89-4-1800A	0.99	0.99
CHS-89-4-1800B	1.00	0.96
CHS-89-4-1800C	1.00	1.00
CHS-89-4-2200A	0.91	0.91
CHS-89-5-1800A	1.03	1.02
CHS-89-5-1800B	1.00	0.96
CHS-89-5-2200A	1.00	0.99
CHS-89-5-2200B	1.02	1.02
CHS-114-4-1800A	1.15	1.15
CHS-114-4-2200A	1.03	0.99
CHS-114-4-2200B	1.06	1.01
CHS-114-5.5-1800A	1.01	0.97
CHS-114-5.5-2200A	1.01	1.00
Mean	1.03	1.02
COV	0.05	0.05

198

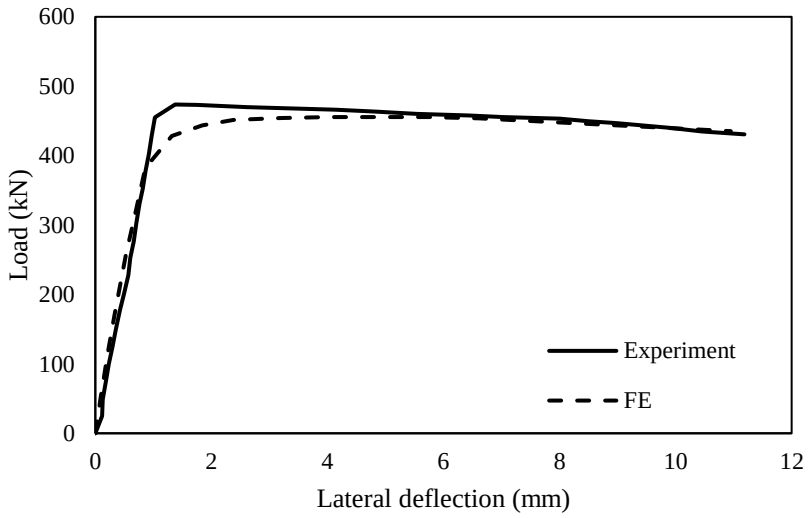

(a) columns (O89-L800-A)

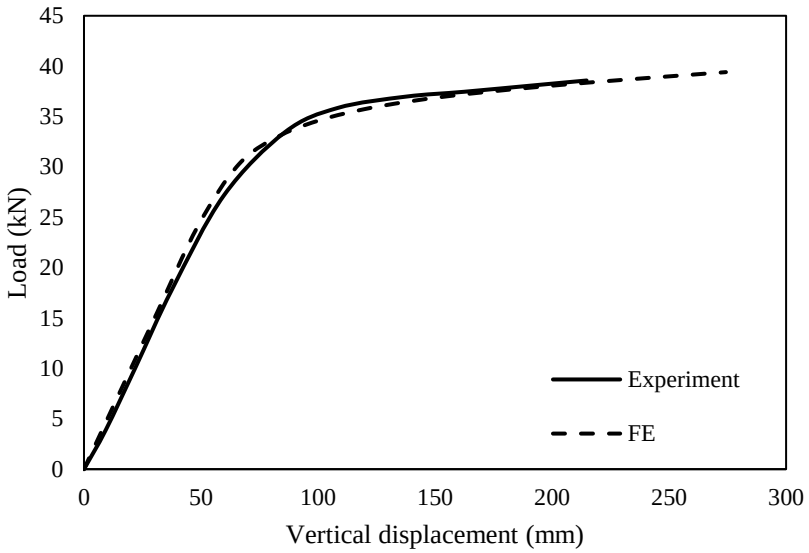

(b) beams (CHS 89-5-2200-A)

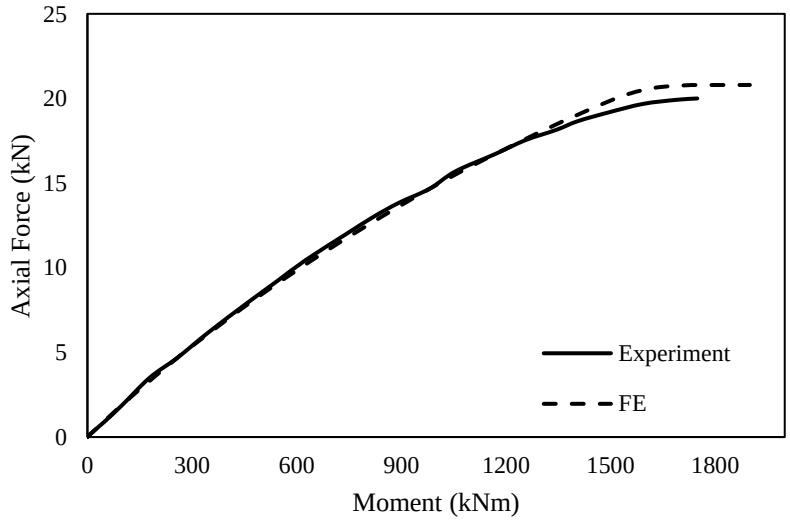

(c) beam-columns (C2L1000E50)

Figure 4: Comparison of experimental and numerical curves for typical cases.

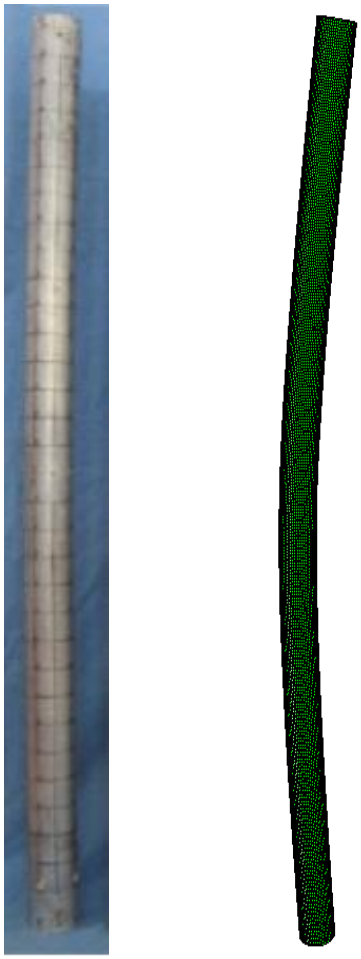

(a) columns (089-L1650-A)

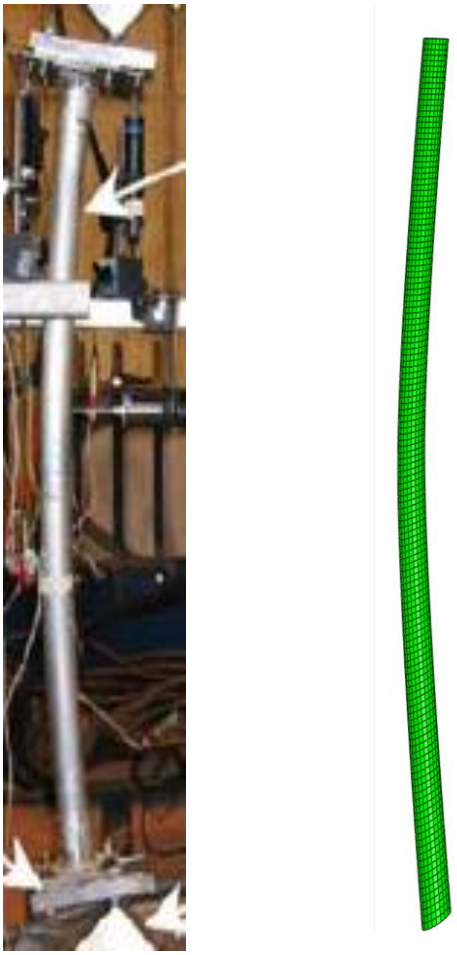

(b) beam-columns (C1L1000E45)

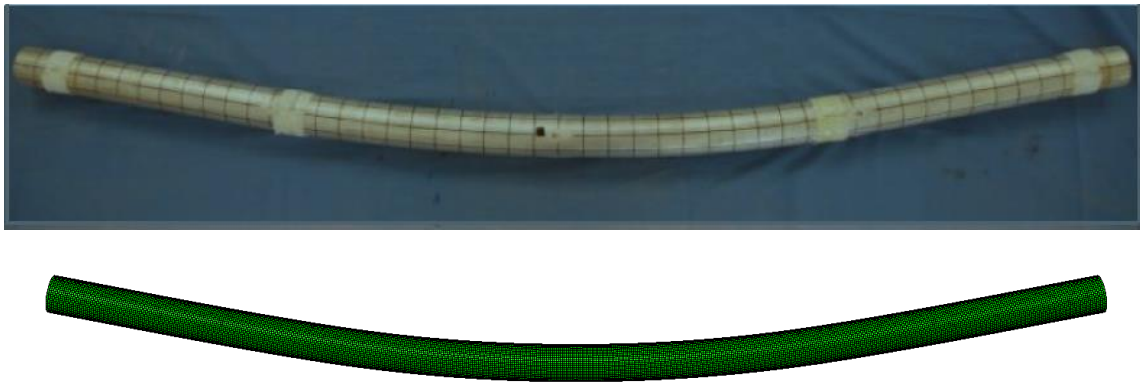

(c) beams (CHA-89-5-2200B)

Figure 5: Comparison of experimental and numerical failure modes.

5. Parametric study

Following the successful validation of the non-linear FE model, a parametric study was conducted on 168 aluminium CHS models with stocky cross-sections. Three cross-sections, four lengths, six eccentricities and a pure bending case, as presented in Table 4, were modelled for each of the two different aluminium alloys (6082-T6 and 6061-T6). Average material properties from those reported in the chosen experimental studies were used for the parametric study, as shown in Figure 6. The member lengths were chosen to obtain a range of member slendernesses, whilst the external diameter was kept constant and equal to 50 mm and the thickness was varied from three to five mm with a step of 1 mm. The eccentricities were varied from zero to 100 mm to provide a range of axial load to bending moment ratios to evaluate the existing design interaction curves for members subjected to a combined axial load and moment (Section 6). The validation results indicated that local and global geometrical imperfection amplitudes of t/10 and L/1000, respectively, led to the most accurate results and were therefore used for the parametric study of the column and beam-column members. In line with the considerations described in Section 4, a local imperfection amplitude of t/10 that ensured an adequate capture of the ultimate load and moment-curvature response was chosen for the beam specimens. These amplitudes have been identified to produce accurate numerical results and have been adopted in previously published numerical studies on thin-walled members made of nonlinear metallic materials, including Wang et al. (2016) and Zhu and Young (2008).

Table 4: List of key parameters included in the parametric study.

Total analyses: 168	
3 cross-sections	• 50×3 • 50×4 • 50×5
2 aluminium alloy materials	• 6082-T6 • 6061-T6
4 lengths	• 300 mm • 600 mm • 900 mm • 1200 mm
7 loading cases	• e: 0 mm (column) • e: 2 mm (beam-column) • e: 5 mm (beam-column)

	• e: 10 mm (beam-column) • e: 25 mm (beam-column) • e: 100 mm (beam-column) • beam

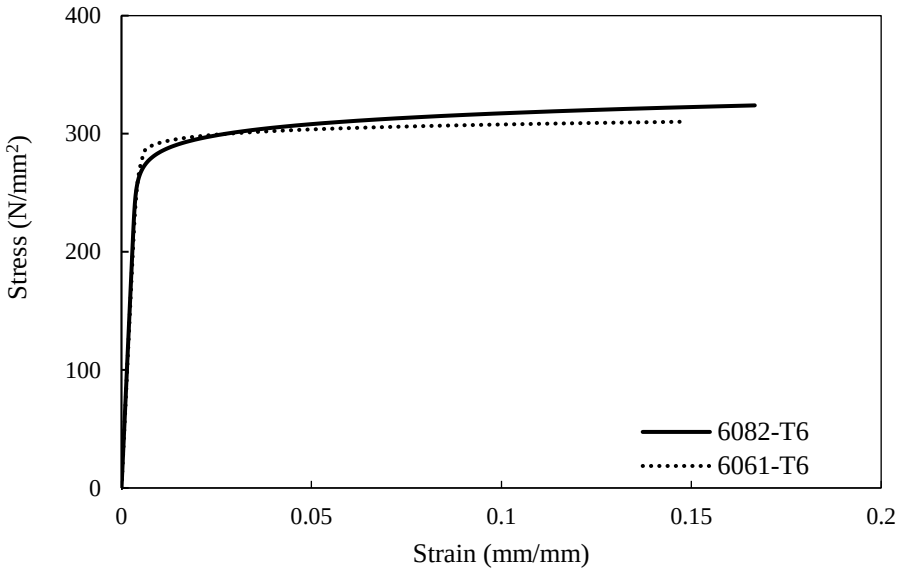

Figure 6: Stress-strain curves used for the parametric study.

A typical example of the obtained load-deflection curves is shown in Figure 7, where the response of a specimen made from 6061-T6 for all four studied lengths is depicted. Note that the labels used in the legend correspond to the type of applied loading: "C" for column and "BC" for beam-column, followed by thickness, length and applied eccentricity. For example, BC-4-300-25 denotes a beam-column member of cross-section 50×4 mm, length of 300 mm and applied eccentricity of 25 mm. Overall the following observations can be made for the parameters studied:

- Material grade: the study focussed on two 6xxx series aluminium alloys with T6 heat treatment that presented similar material response, as shown in Figure 6. This has led to similar performance of the two studied alloys, as will also be quantitively demonstrated in Section 6.
- Member length: As anticipated, the ultimate load decreased with increasing member length, for example the ultimate capacity of 300 mm member with e=10 mm is equal to 100.54 kN (see Figure 7(a)), whilst it falls to 59.41 kN and (see Figure 7(c)) for a 900 mm member with the same eccentricity.

- Applied eccentricities: Based on Figures 7(a)-7(d), it can generally be observed that the specimens subjected to small loading eccentricities (0, 2, 5, 10 mm) reached their peak load with minimal deflections before a rapid loss of stiffness occurred, causing extensive deformations as the load reduced due to the member failing by flexural buckling. Specimens subjected to a larger eccentric load (e.g., 25, 100 mm) generally reached their peak loads much later than their counterparts and presented a smoother load descending curve for increasing deformations.
- Cross-sections: The study included only stocky cross-sections that are not prone to local buckling effects. As anticipated, higher load and moment capacities have been observed in cross-sections with larger thickness. For example, the member BC-5-300-25 of 6082-T6 presented ultimate load equal to 76.9 kN, whilst for the same member of 3 mm thickness (BC-3-300-25), the ultimate numerically achieved load was equal to 49.2 kN.

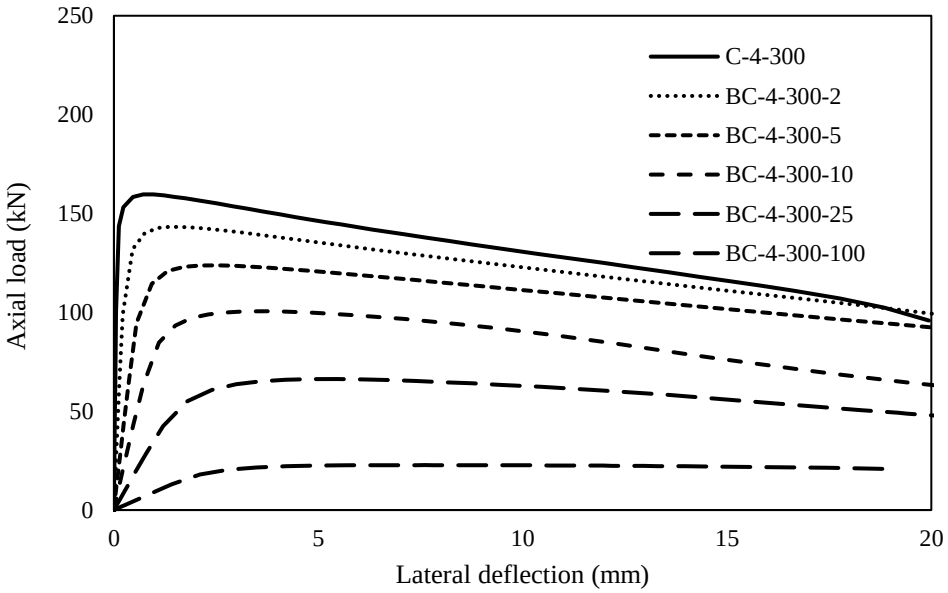

(a) Length: 300 mm

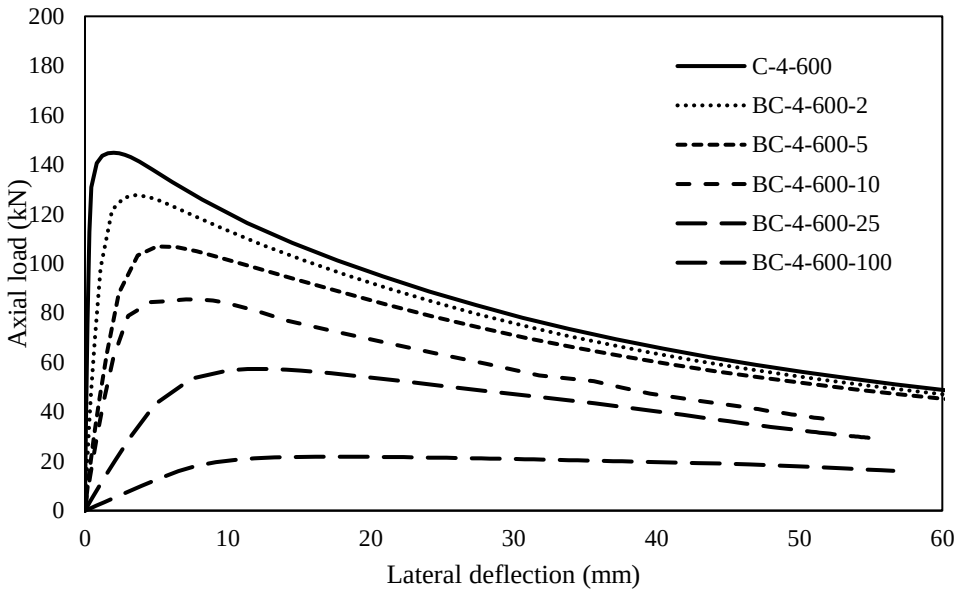

(b) Length: 600 mm

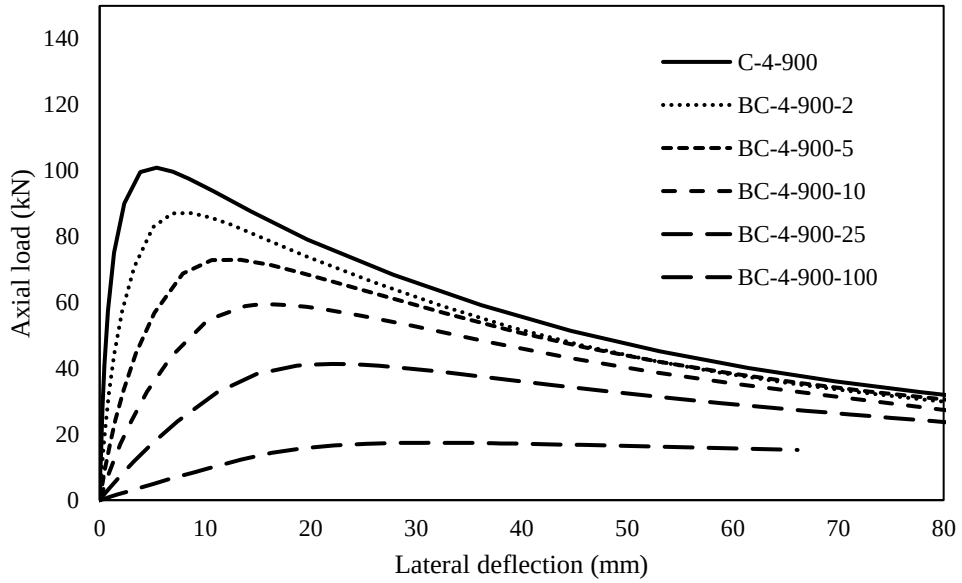

(c) Length: 900 mm

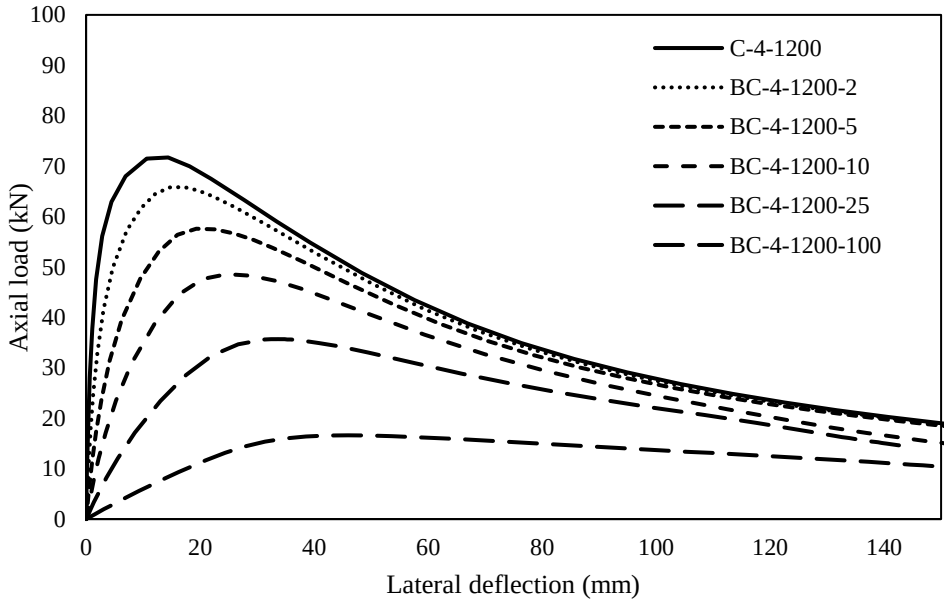

(d) Length: 1200 mm

Figure 7: Typical parametric study results (material: 6061-T6, cross-section: 50×4).

6. Assessment of design guidelines

The numerically obtained capacities are utilised in this section to assess and compare the accuracy of the following design predictions: European design provisions, Direct Strength Method, Aluminium Design Manual. All safety factors are set to unity. The design strengths for both 6061-T6 and 6082-T6 aluminium alloy beam-columns were calculated using the predicted strengths ($M_{pred,}$ N_{pred}) and then compared with the numerically obtained ones. In order to allow for a more direct assessment, the ratio R of the beam-column specimens can be established. In Figure 8, the bending moment capacity normalised with the predicted one (M/M_{pred}) is plotted against the axial compressive capacity normalised with the predicted one (N/N_{pred}), with both ratios being equal to unity at their intersection with the respective axis. In the same figure, it is also included the design interaction curve that links the two extremes (i.e., from pure bending at vertical axis to pure compression at horizontal axis), as well as a FE result (N_u, M_u). Note that for test/FE points above the design interaction curve indicate an overconservative design estimation; points below the design curve indicates unsafe predictions, whilst highest accuracy in predicted capacity is achieved when the test/FE points are closer to the curve. The capacity ratio R which is used in the assessments hereafter, represents the distance from the upper end of the straight line extending from the origin (0,0) to (N_u, M_u) and the intersection of this line with the design interaction curve. The angle (θ)

can also be defined to indicate the ratio of the combined axial compression and bending moment applied to the specimen (the two extremes being: θ = 0°, which shows that the specimen is subjected to pure bending, and θ = 90°, which shows that the specimen is subjected to axial compression). In addition to the 168 FE data of the parametric study shown in Section 5, the assessment hereafter utilises the 34 experimental data, reported at Wang et al. (2015), Zhu and Young (2006), Feng et al. (2020) and Zhao and Zhai (2020).

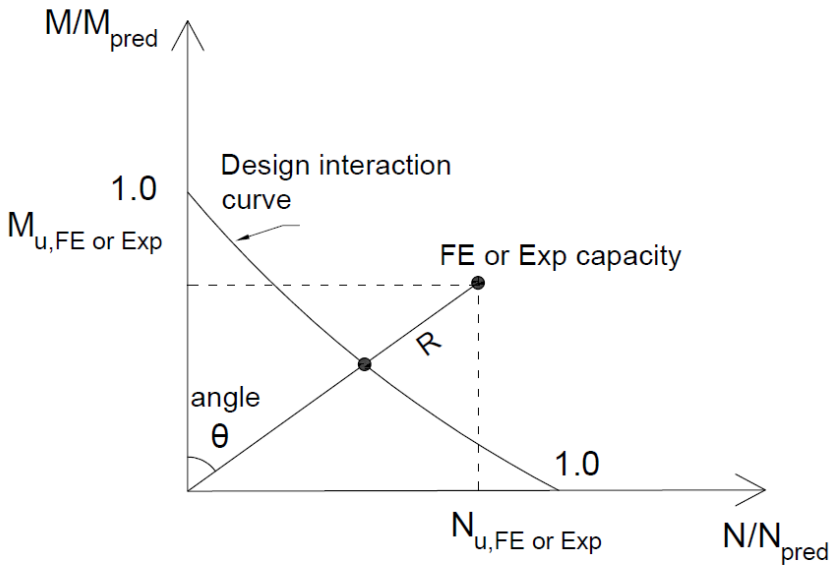

Figure 8: Design interaction curve – definition of R and θ.

6.1 European design provisions

In order to estimate the resistance of aluminium alloy beam-column members, EN 1999-1-1 (2007) suggests an interaction formula between the buckling resistance and bending resistance of a member.

The calculation of the buckling resistance (N_{EC9}) of an aluminium alloy member is defined by Equation (1)

$$N_{EC9} = \chi A \sigma_{0.2} \quad (1)$$

Where χ is the buckling reduction factor, A is the gross area of the cross-section, and $\sigma_{0.2}$ is the characteristic yield/proof strength of the material. The reduction coefficient χ is given by Equation (2).

$$\chi = \frac{1}{\varphi + \left[\varphi^2 - \bar{\lambda}^2\right]^{0.5}} \leq 1.0 \quad (2)$$

292 The parameter φ can be estimated by Equation (3)

$$\varphi = 0.5\left[1 + \alpha\left(\bar{\lambda} - \bar{\lambda}_0\right) + \bar{\lambda}^2\right] \quad (3)$$

293 where α and $\bar{\lambda}_0$ is the imperfection factor and the limit of the horizontal plateau, respectively,
294 corresponding to the relevant buckling curve (for 6082-T6, 6061-T6: α is 0.2 and $\bar{\lambda}_0$ is 0.1) The
295 member slenderness $\bar{\lambda}$ is given by Equation (4)

$$\bar{\lambda} = \sqrt{\frac{A\sigma_{0.2}}{N_{cr}}} \quad (4)$$

296 where N_{cr} is the elastic critical buckling load of the column, based on the gross cross-sectional
297 properties. Note that all considered cross-sections were Class 1-2, based on the slenderness
298 limits specified in EC9, and thus the remaining classes are out of the scope of the present study.

299 Using the 24 FE data of the members subjected to pure compression and 8 experimental
300 data from Wang et al. (2015), the accuracy of the Eurocode buckling curve (i.e., Equations (2)-
301 (3)) can be assessed. In Figure 9, the ultimate loads (N_u) are normalised by the squash load
302 ($A\sigma_{0.2}$) and plotted against the member slenderness $\bar{\lambda}$ As can be seen, the EC9 buckling curve
303 appears to generally predict well the buckling loads.

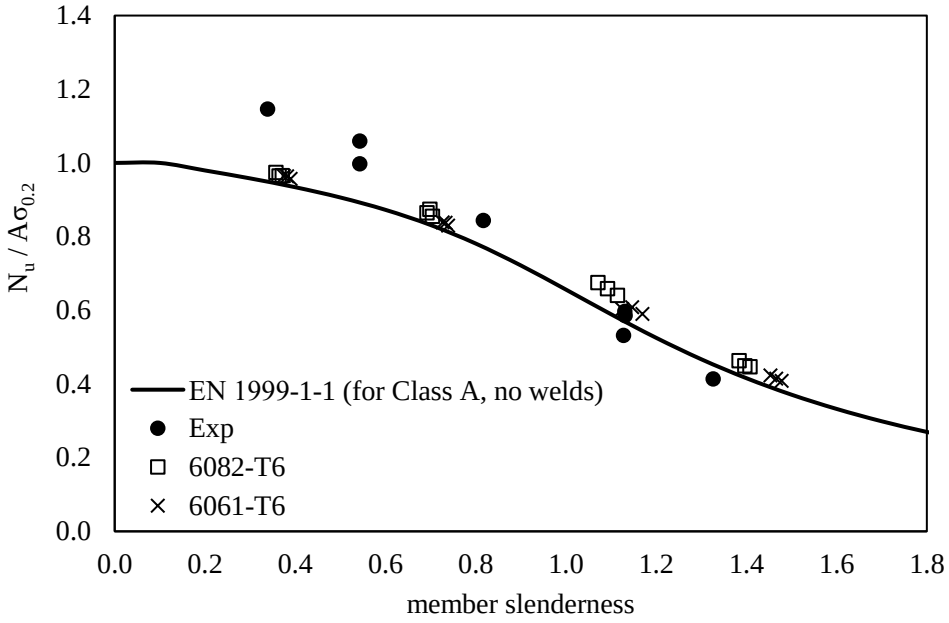

304

305 Figure 9: Assessment of EC9 buckling curve.

306 For the calculation of the bending resistance (M_{EC9}) of the members, EC9 specifies Equation
307 (5):

$$M_{EC9} = \alpha \sigma_{0.2} W_{el} \quad (5)$$

308 Where α, is the shape factor and W_{el} is the elastic modulus of the cross-section.

309 The predicted axial and flexural resistances of the members (N_{EC9} and M_{EC9}) were used to
310 produce the normalised axial load and bending moments that will be compared to the
311 interaction curve (see Equation (6)):

$$\left[\left(\frac{N_u}{N_{EC9}}\right)^{\psi_c} + \left(\frac{M_u}{M_{EC9}}\right)^{1.7}\right]^{0.6} \leq 1.00 \quad (6)$$

312 Note that EC9 provides two alternative procedures for the evaluation of parameter ψ_c: ψ_c
313 (which should be ≥0.8) equals to either 1.3χ for Class 1 and Class 2 cross-sections and
314 ψ_c=ψ(=1.00) for Class 3 and Class 4 sections (Method A, hereafter), or alternatively, ψ_c may
315 be taken as 0.8 for all cross-sections (Method B, hereafter). All relevant interaction curves are
316 presented for comparison purposes in Figure 10, where it can be seen that for Method A, the
317 curve varies based on the reduction parameter χ (i.e., based on the member's slenderness),

whilst for $\chi \geq 0.61$ the curve coincides with that of Method B, where ψ_c is always considered equal to 0.8.

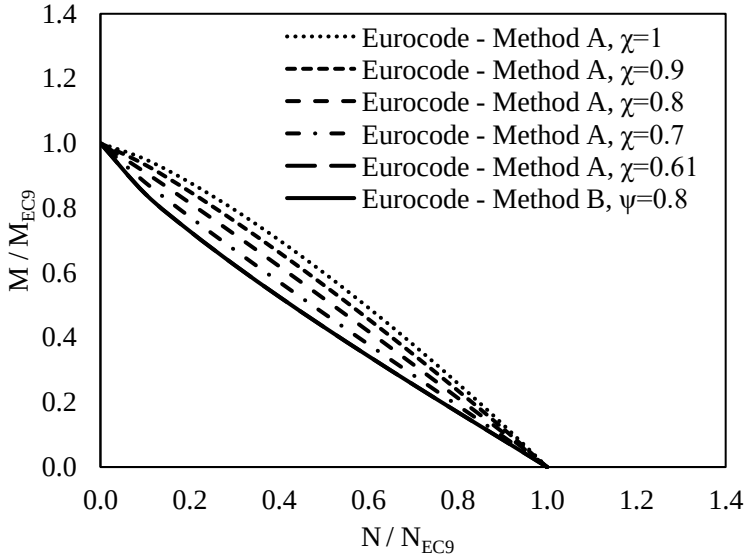

Figure 10: Eurocode curves (Method A: ψ_c as a function of χ for Classes 1-2, Method B: ψ_c=0.8 for all Classes)

In Figure 11, the ultimate performance is normalised by the resistances predicted by EC9 and plotted in the form of M-N interaction curves. In the same graph, the Eurocode curve with Method B (which is constant for all studied specimens) is included. It should be noted that data points slightly above the interaction curve show safe predictions. Moving further above the line, predictions are conservative, whilst points below the curve correspond to unsafe predictions. As shown, the data points lie fairly close to the curve with satisfactory consistency, demonstrating accurate predictions. Similar conclusions can be drawn from Figure 12 and Table 5, where the results are also presented for the two studied materials, but also separately for Methods A and B. It can also be observed that for Method A, for which the parameter ψ_c is a function of the slenderness parameter, the accuracy improves (mean: 1.01 for Method A, mean: 1.05 for Method B). In Table 5, the results are also reported based on the considered lengths. The predicted capacity ratios appear more accurate for Method A compared to Method B for specimens of lengths 300 mm and 600 mm, but are the same for longer specimens. This is in line with the limitation of Method A to have $\psi_c \geq 0.8$ (which correponds to $\chi \geq 0.61$), that leads to same accuracy values for specimens of length 900 mm and 1200 mm. The trend is similar for both examined aluminium alloy grades.

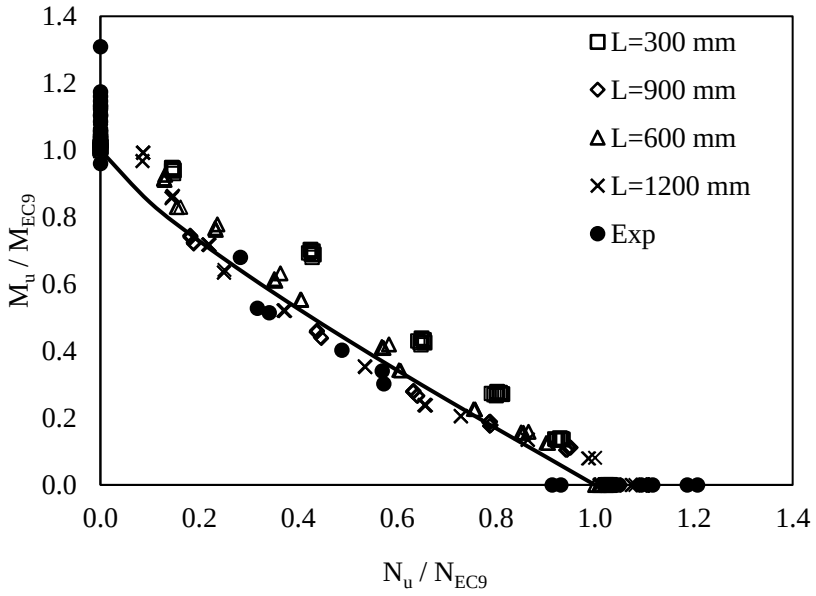

339 Figure 11: Ultimate performance normalised with EC9 strength for the two numerically
340 studied materials (Design Interaction curved based on Method B).

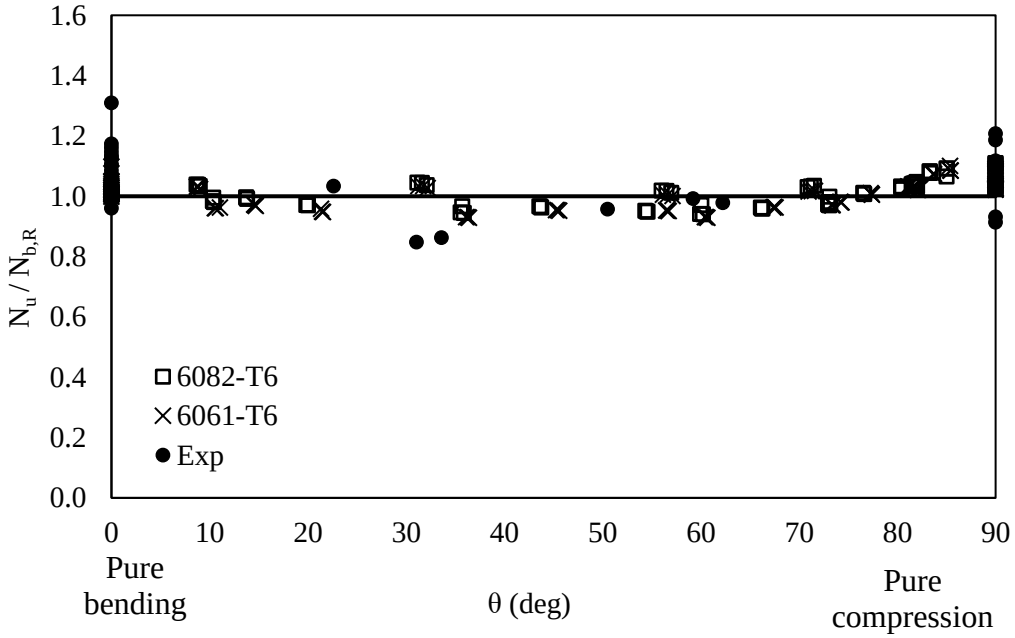

a) EC9 – Method A

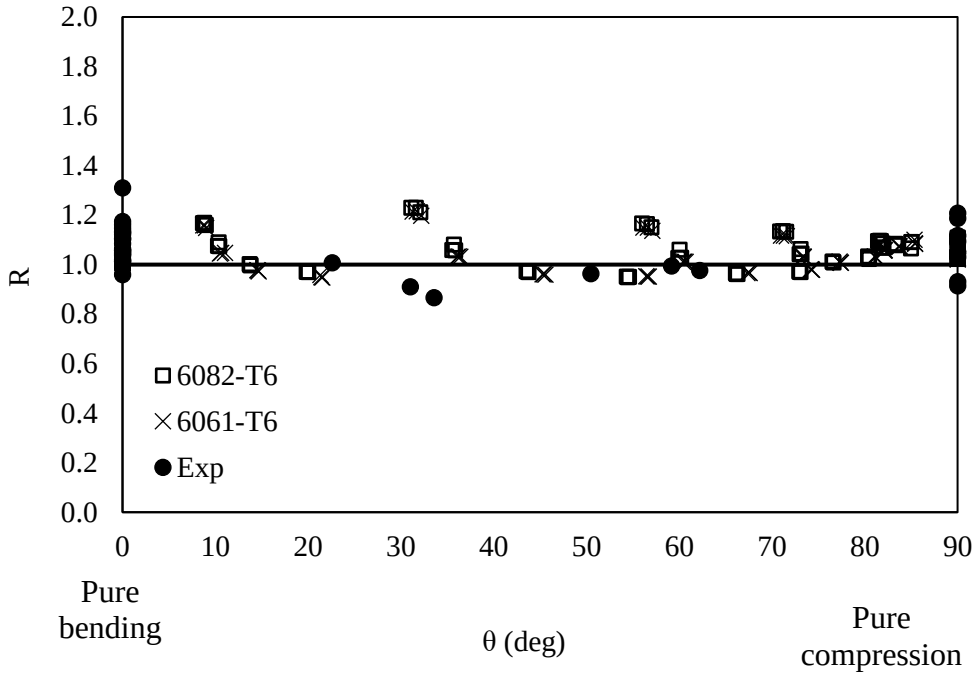

b) EC9 – Method B

341 Figure 12: Assessment of Eurocode; results presented with respect to degree θ of
342 compression/bending.

343 Table 5: Assessment of Eurocode 9 - Accuracy R; for the two studied materials.

		Eurocode - Method A				Eurocode - Method B			
		6082-T6		6061-T6		6082-T6		6061-T6	
Specimen	No FE/exp	mean	COV	mean	COV	mean	COV	mean	COV
C/BC/B-3-300	14	1.03	0.01	1.02	0.01	1.11	0.07	1.10	0.06
C/BC/B -4-300	14	1.03	0.01	1.02	0.01	1.12	0.07	1.11	0.06
C/BC/B -5-300	14	1.03	0.01	1.02	0.01	1.12	0.07	1.04	0.02
C/BC/B -3-600	14	0.99	0.04	0.98	0.04	1.04	0.02	1.03	0.02
C/BC/B -4-600	14	1.01	0.03	0.98	0.04	1.06	0.03	1.03	0.02
C/BC/B -5-600	14	0.99	0.04	0.98	0.05	1.04	0.02	1.03	0.01
C/BC/B -3-900	14	1.02	0.06	1.00	0.05	1.02	0.05	1.01	0.04
C/BC/B -4-900	14	1.02	0.06	1.01	0.05	1.02	0.05	1.02	0.05
C/BC/B -5-900	14	1.02	0.05	1.02	0.06	1.02	0.05	1.02	0.06
C/BC/B-3-1200	14	1.01	0.05	1.02	0.06	1.01	0.05	1.02	0.06
C/BC/B-4-1200	14	1.01	0.05	1.02	0.06	1.02	0.05	1.02	0.06
C/BC/B-5-1200	14	1.02	0.06	1.02	0.06	1.02	0.06	1.02	0.06
All FE (each grade)		1.01	0.04	1.01	0.05	1.05	0.06	1.04	0.06
Collated Exp	34		mean 1.02	COV 0.06			mean 1.05	COV 0.06	
All (FE and Exp)	202		mean 1.01	COV 0.04			mean 1.05	COV 0.07	

6.2 Direct Strength Method (DSM)

The DSM can be considered as a generalised slenderness method for structural design and was originally developed for cold formed steel sections (Schafer, 2008). The method aims to overcome the complexity and limitations of the effective width method and combines the interaction of local, flexural and distortional buckling of thin-walled members. The latter is not discussed in this paper, as it is not relevant for the presently studied circular hollow sections.

Research has been carried out to extend the method's application to aluminium alloy sections by Zhu and Young (2006b, 2009) and the applicability of the expressions proposed in the aforementioned studies is examined hereafter. According to them, the axial strength of the member (N_{DSM}) is calculated as the minimum between the overall flexural buckling (N_{ne}) and the local buckling (N_{nl}) strength. Equations (8), (9) are recommended to estimate these strengths, where N_y is the yield load and is equal to $A\sigma_{0.2}$, $\lambda_l = \sqrt{N_{ne}/N_{crl}}$, with N_{crl} being the critical elastic local buckling load, $\lambda_c = \sqrt{N_y/N_{cre}}$, where N_{cre} is the critical elastic flexural buckling load. In a similar way, the bending strength of a member is the minimum between the nominal flexural strength for lateral-torsional buckling (M_{ne}) and the nominal flexural strength for local buckling (M_{nl}), which are calculated from Equations (11) and (12), respectively. In these equations, M_y is equal to $\sigma_{0.2}S_g$, where S_g is the elastic cross-sectional modulus (i.e., referring to the extreme fibre in first yield), whilst $\lambda_l = \sqrt{M_{ne}/M_{crl}}$, with M_{crl} being the critical elastic local buckling moment. Upon calculation of these strengths, a linear interaction formula, as shown in Equation (13) is recommended for members subjected to combined axial compression and bending moment. Note that for the evaluation of N_{crl} and M_{crl}, the elastic local buckling stress (f_{crl}) provided in Equation (14) has been used, both for the case of compression and of bending (Buchanan et al., 2019), where v the material's Poisson's ratio.

$$N_{DSM} = \min(N_{ne}, N_{nl}) \tag{7}$$

$$N_{ne} = \begin{cases} (0.658^{\lambda_c{}^2})\, N_y & \text{for } \lambda_c \le 1.5 \\ (0.877/\lambda_c{}^2)\, N_y & \text{for } \lambda_c > 1.5 \end{cases} \tag{8}$$

$$N_{nl} = \begin{cases} N_{ne} & \text{for } \lambda_l \le 0.713 \\ \left[1 - 0.15\left(\frac{N_{crl}}{N_{ne}}\right)^{0.3}\right]\left(\frac{N_{crl}}{N_{ne}}\right)^{0.3} N_{ne} & \text{for } \lambda_l > 0.713 \end{cases} \tag{9}$$

$$M_{DSM} = \min(M_{ne}, M_{nl}) \tag{10}$$

$$M_{ne}=\begin{cases} M_{cre} & \text{for } M_{cre} < 0.56M_y \\ \left(\frac{10}{9}\right) M_y \left(1-\frac{10M_y}{36M_{cre}}\right) & \text{for } 0.56M_y \le M_{cre} \le 2.78M_y \\ M_y & \text{for } M_{cre} > 2.78M_y \end{cases} \quad (11)$$

$$M_{nl}=\begin{cases} M_{ne} & \text{for } \lambda_l \le 0.713 \\ [1-0.15\left(\frac{M_{crl}}{M_{ne}}\right)^{0.3}]\left(\frac{M_{crl}}{M_{ne}}\right)^{0.3} M_{ne} & \text{for } \lambda_l > 0.713 \end{cases} \quad (12)$$

$$\left(\frac{N_{u,FE}}{N_{DSM}}\right)+\left(\frac{M_{u,FE}}{M_{DSM}}\right) \le 1.00 \quad (13)$$

$$f_{crl} = \frac{E}{\sqrt{3(1-v^2)}}\frac{2t}{D} \quad (14)$$

The numerically obtained strengths are used to evaluate the accuracy of the DSM for aluminium alloy circular hollow section members. Note that for the members investigated herein $\lambda_c \le 1.5$ ($0.36 \le \lambda_c \le 1.48$) as the study did not focus on very slender members, whilst due to the low value of local slenderness, $\lambda_l \le 0.713$ ($0.12 \le \lambda_l \le 0.24$), local buckling was not a primary failure mode. In addition, distortional buckling does not occur in CHS sections and lateral-torsional buckling was not an observed failure mode.

Firstly, the data for the cases of pure compression and of pure bending are utilised to assess the predicted strengths for the two extreme cases. This is presented in Figure 13, where the ultimate loads (N_u) are normalised with the predicted strengths calculated using Equations (7)-(9) (N_{DSM}) and plotted against the column slenderness. It can be seen that N_{DSM} can generally predict well the buckling strength. On the other hand, the method which was initially formulated for thin-walled structures, does not consider any plastic bending moment, even for sections with low cross-section slenderness values, as those studied herein. Hence, as shown in Figure 13(b), the flexural strength of stocky CHS aluminium sections is clearly underestimated by the DSM equation (i.e., M_u/M_{DSM} well over unity). In the same figure, the moment capacities have also been normalised with the plastic moment resistance (M_{pl}), which is evaluated multiplying the plastic section modulus with the material's proof strength, and as can be observed, this leads to accurate flexural strength predictions.

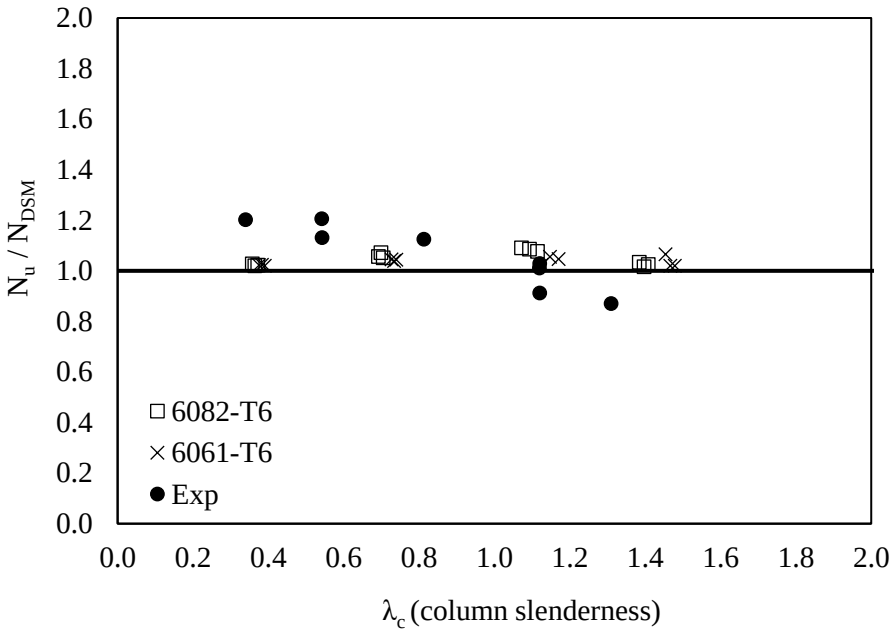

(a) Buckling strength, based on 24 FE data of columns and 8 experimental reported column data

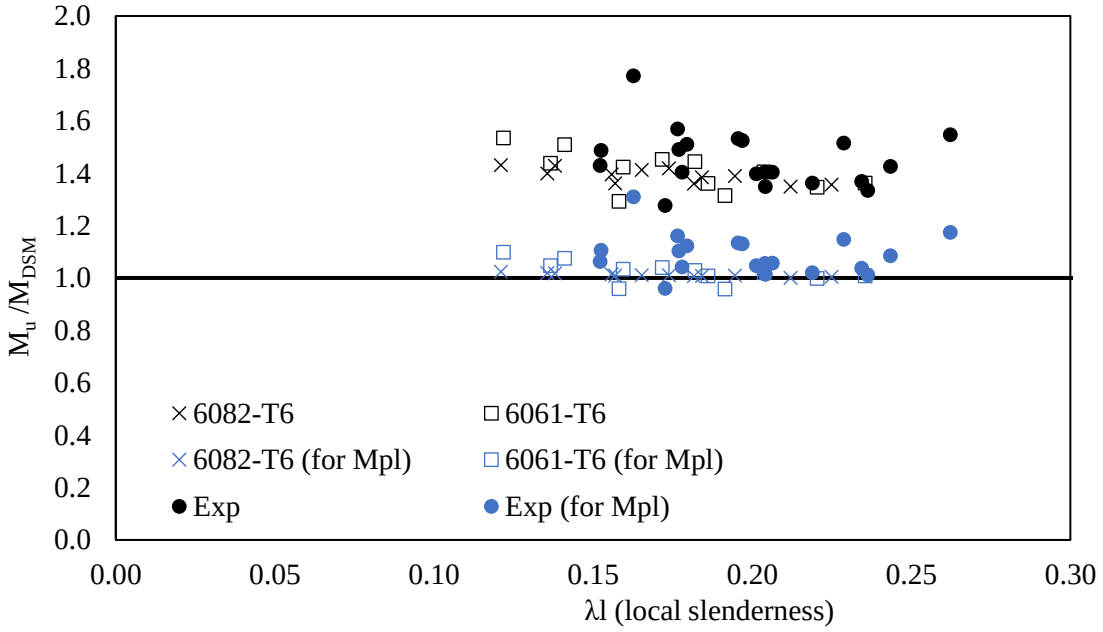

(b) Flexural strength, based on 24 FE data of beams and 20 experimental reported beam data

Figure 13: Assessment of DSM predicted strengths for the cases of pure compression and pure bending.

To evaluate the DSM recommendation for beam-columns (i.e., Equation (13)), Figure 14(a) presents the ultimate strengths normalised with DSM predictions and presented

together with the linear interaction curve. The results are shown with different markers according to their length. As can be seen, for members subjected to a combination with higher bending moment, the prediction is less accurate, as the normalised points diverge from the interaction curve. This is mainly related to the conservative M_{ne} prediction, which does not consider the plastic moment resistance achieved by stocky sections. To eliminate this conservatism, the plastic moment resistance should be used in place of the elastic one. Figure 14(b) presents the data normalised with the DSM buckling strength for the N capacities (N_u/N_{DSM}) and with the plastic resistance for the M capacities (M_u/M_{pl}). On the basis of normalised data, the interaction curve shown in Figure 14 and expressed in Equation (15), is recommended in order to capture the response of aluminium alloy CHS beam-columns with stocky cross-sections ($\lambda_l \leq 0.30$).

$$\left[\left(\frac{N_u}{N_{DSM}}\right)^{0.8} + \left(\frac{M_u}{M_{pl}}\right)\right] \leq 1.00 \quad (15)$$

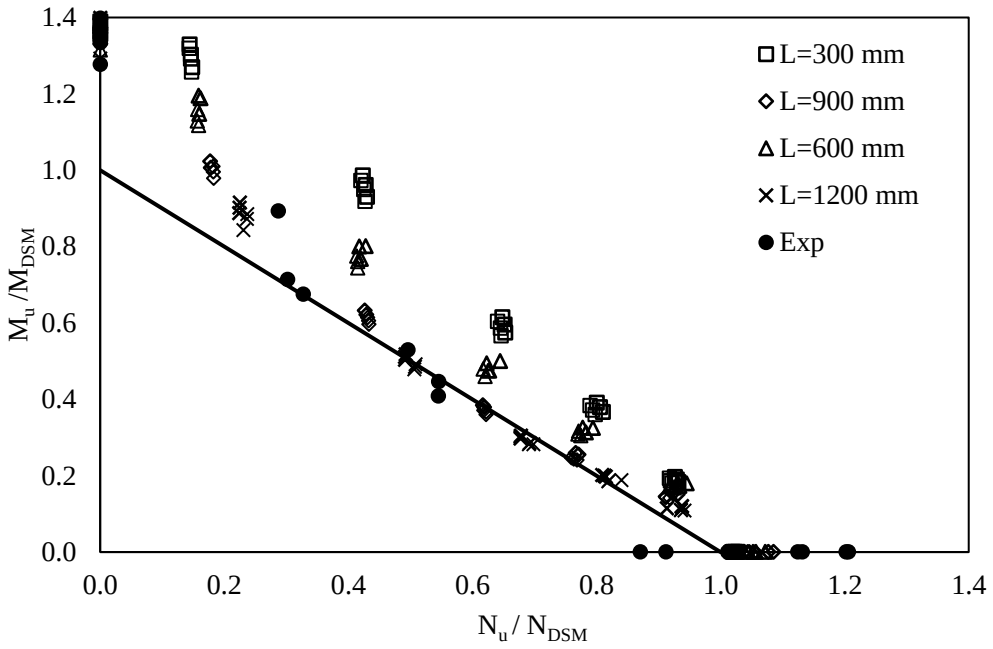

(a) Ultimate performance normalised with DSM strength - Design interaction curve based on DSM.

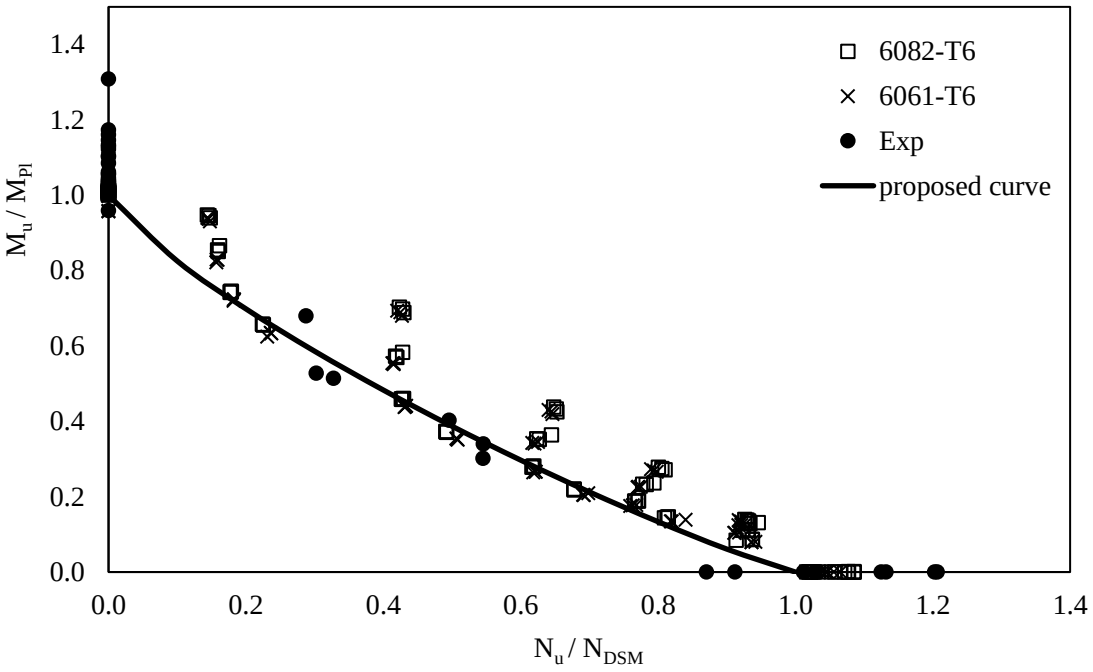

(b) Ultimate performance normalised with N_{DSM} and M_{Pl} - Proposed interaction curve

Figure 14: Ultimate performance normalised with DSM strength for the two numerically studied materials.

The linear interaction curve and the proposed interaction curve for stocky cross-sections, are further assessed in Figure 15 and Table 6. As shown in Figure 15(a), the DSM predictions appear less accurate and more scattered, compared to Figure 15(b). Similar conclusions are drawn from Table 6, where the predicted capacities ratios show similar performance for the two aluminium alloys. A mean value of R equal to 1.16 has been achieved for the two studied materials for the DSM. The proposed modification for stocky cross-sections significantly improves the R value to 1.04. In addition, the scatter reduces and thus the COV which was relatively high for DSM (COV=0.15) improves using the proposed modification (COV=0.07).

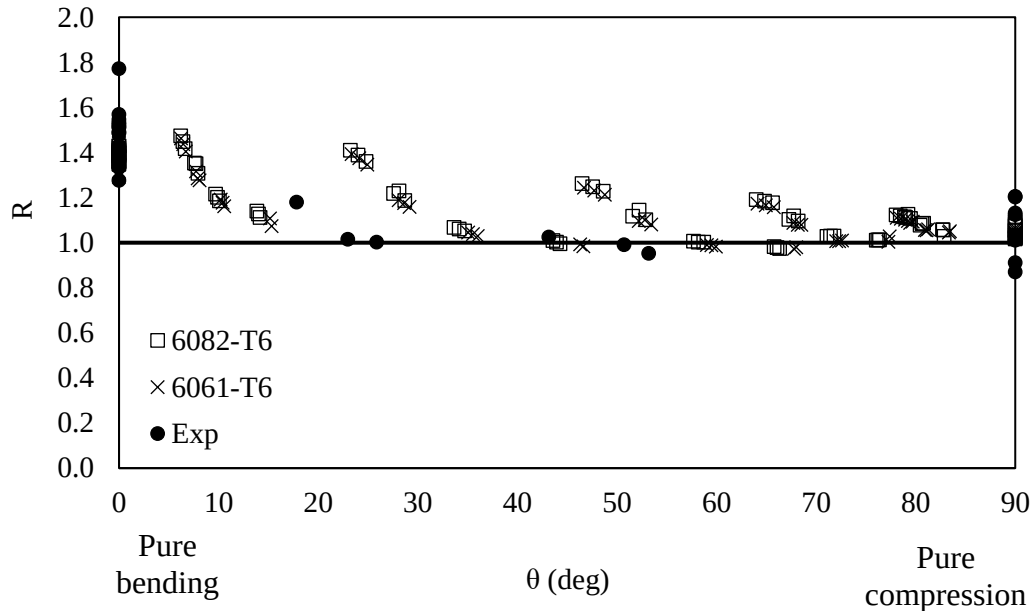

(a) Based on DSM strengths

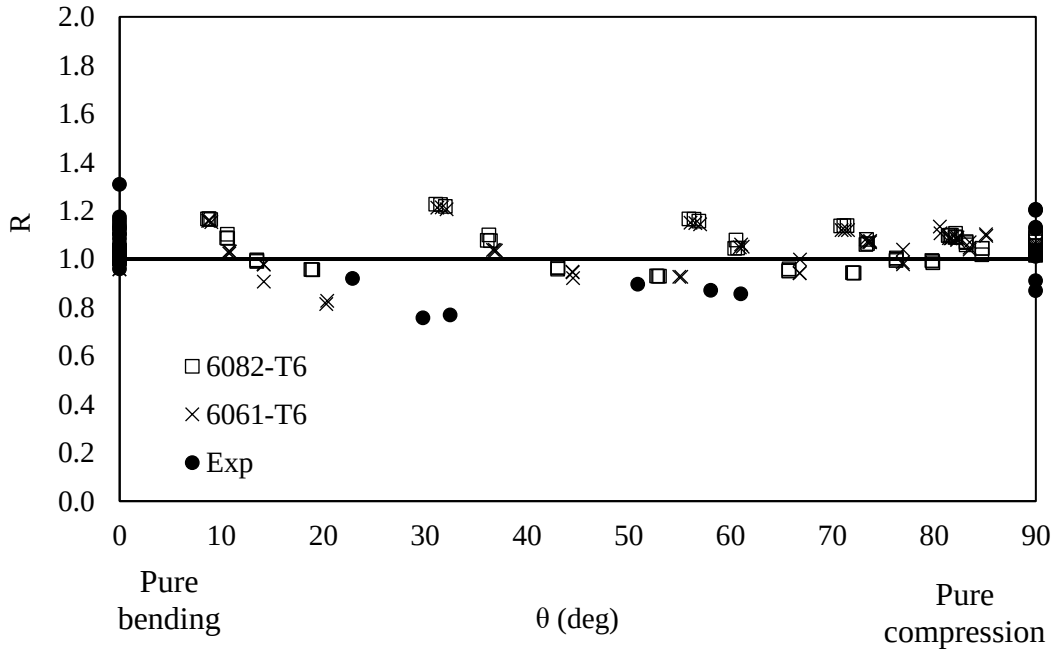

(b) Based on N_{DSM}, M_{pl} and proposed interaction curve

411 Figure 15: Assessment of DSM and of the proposed modification for stocky cross-
412 sections; results presented degree θ of compression/bending.

413

Table 6: Assessment of DSM and of the proposed modification for stocky cross-sections Accuracy R; for the two studied materials.

		DSM				Proposal for stocky cross-sections			
		6082-T6		6061-T6		6082-T6		6061-T6	
Specimen	No FE	mean	COV	mean	COV	mean	COV	mean	COV
C/BC/B-3-300	14	1.24	0.12	1.23	0.12	1.12	0.07	1.11	0.06
C/BC/B -4-300	14	1.26	0.13	1.25	0.13	1.12	0.07	1.11	0.06
C/BC/B -5-300	14	1.27	0.13	1.26	0.14	1.12	0.07	1.11	0.06
C/BC/B -3-600	14	1.17	0.10	1.15	0.10	1.06	0.03	1.04	0.02
C/BC/B -4-600	14	1.20	0.10	1.15	0.09	1.08	0.03	1.04	0.04
C/BC/B -5-600	14	1.20	0.12	1.18	0.13	1.06	0.03	1.05	0.02
C/BC/B -3-900	14	1.12	0.11	1.09	0.12	1.01	0.05	0.99	0.04
C/BC/B -4-900	14	1.12	0.12	1.11	0.14	1.01	0.05	1.00	0.05
C/BC/B -5-900	14	1.13	0.13	1.12	0.16	1.01	0.05	1.00	0.06
C/BC/B-3-1200	14	1.07	0.12	1.07	0.10	0.98	0.04	0.98	0.06
C/BC/B-4-1200	14	1.08	0.14	1.08	0.15	0.99	0.04	0.99	0.05
C/BC/B-5-1200	14	1.09	0.14	1.10	0.18	0.99	0.05	0.99	0.06
All FE (each grade)		1.16	0.13	1.15	0.13	1.04	0.07	1.03	0.07
Collated Exp	34		mean 1.29	COV 0.18			mean 1.04	COV 0.12	
All (FE and Exp)	168		mean 1.18	COV 0.15			mean 1.04	COV 0.07	

6.3 Aluminium Design Manual

The design recommendations of the Aluminium Design Manual (Aluminum design manual, 2015) for the aluminium alloy members are assessed in this section. The design strengths for axial compression (N_{AA}) are defined as the minimum among the states of member buckling N_{cm}, local buckling N_{cl} and interaction between member buckling and local buckling N_{ce}. N_{cm} is given by Equation (17), where F_c is the compressive yield strength, B_c and C_c are the member buckling constant intercepts, and D_c is the member buckling constant slope, as defined in AA (2015). The bending strength is the minimum between the yielding, rupture ($M_{np,u}$), local buckling (M_{nlb}), and the lateral–torsional buckling (M_{nmb}). The yield bending moment was the failure moment for the sections examined in this study. Formulae for their evaluation of all cases are provided in AA (2015). When a member is subjected to combined axial compression and bending among two axes (y and z), the linear interaction formula given in Equation (19) is recommended.

Only one bending axis was considered in this numerical investigation and hence the bending moment on the other axis is zero.

$$N_{AA} = \min(N_{cm},\ N_{cl},\ N_{ce}); \tag{16}$$

$$N_{cm} = F_c A_g = A_g \begin{cases} F_{cy} \text{ for } \lambda \le \lambda_l = (B_c - F_{cy})/D_c \\ B_c - D_c\lambda\,(0.85 + 0.15(C_c - \lambda)/(C_c - \lambda_l)) \text{ for } \lambda_l \le \lambda \le C_c \\ 0.85\,\pi^2 E/\lambda^3 \text{ for } \lambda \le C_c \end{cases} \tag{17}$$

$$M_{AA} = \min(M_{np,u}, M_{nlb,} M_{nmb}) \tag{18}$$

$$\left|\left(\frac{N_{u,FE}}{N_{AA}}\right) + \left(\frac{M_{u,FE}}{M_{AA,y}}\right) + \left(\frac{M_{u,FE}}{M_{AA,z}}\right)\right| \le 1.00 \tag{19}$$

The accuracy of AA (2015) is assessed in Figure 16, Figure 17 and in Table 7. Similar to the DSM and due to the inaccurate prediction of the bending moment, the interaction design strength appears quite conservative, particularly for members primarily under bending moment. The method leads to R with a mean value of 1.14, with COV equals to 0.18 for both aluminium alloys. This observation is in line with the outcomes reported for rectangular hollow section aluminium alloy beam-columns in Hu et al. (2020).

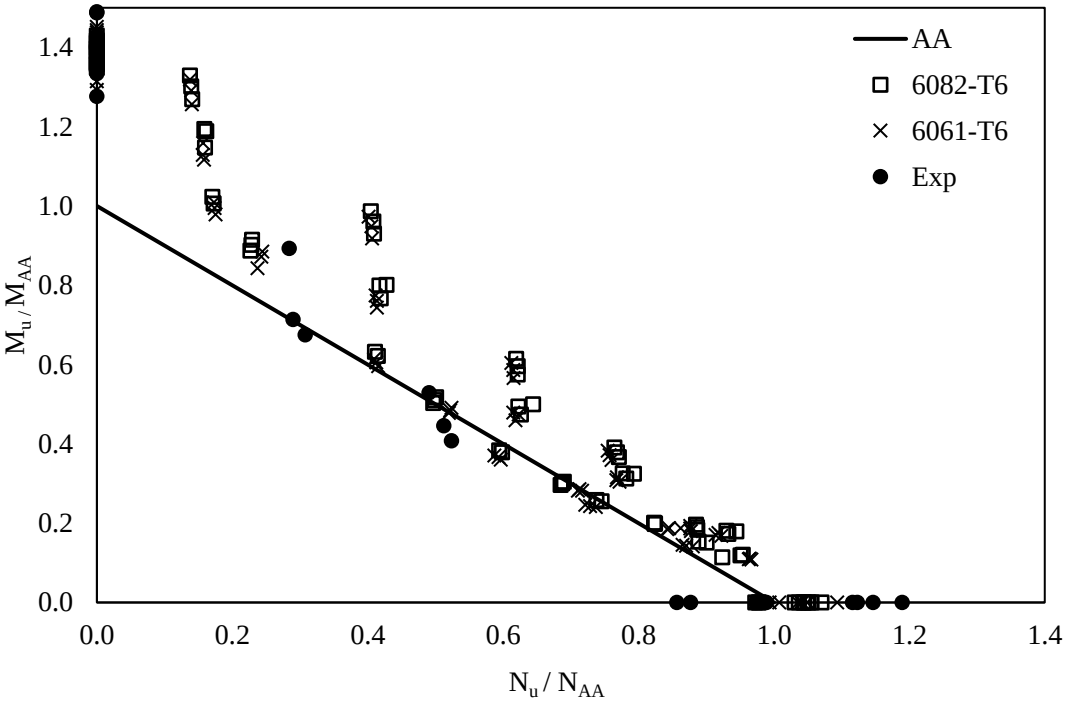

Figure 16: Ultimate performance normalised with AA strength for the two numerically studied materials (Design curve based on AA).

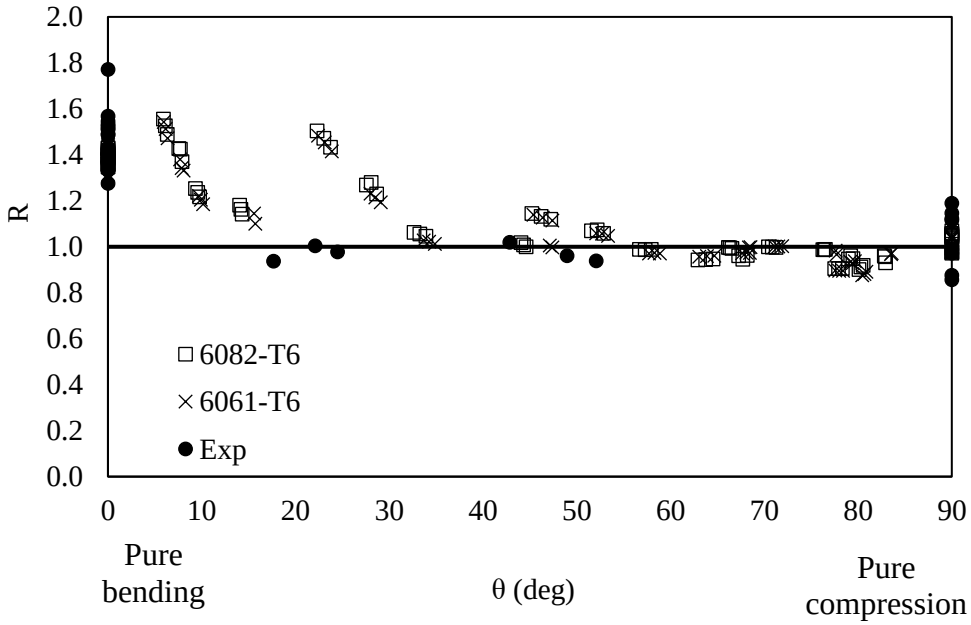

Figure 17: Assessment of AA; results presented degree θ of compression/bending.

Table 7: Assessment of AA - Accuracy R; for the two studied materials.

		6082-T6		6061-T6	
		mean	COV	mean	COV
C/BC/B-3-300	14	1.18	0.21	1.17	0.21
C/BC/B -4-300	14	1.19	0.22	1.19	0.22
C/BC/B -5-300	14	1.21	0.23	1.21	0.23
C/BC/B -3-600	14	1.14	0.15	1.12	0.15
C/BC/B -4-600	14	1.16	0.17	1.12	0.15
C/BC/B -5-600	14	1.16	0.18	1.15	0.18
C/BC/B -3-900	14	1.08	0.14	1.06	0.15
C/BC/B -4-900	14	1.09	0.15	1.07	0.17
C/BC/B -5-900	14	1.10	0.17	1.09	0.20
C/BC/B-3-1200	14	1.07	0.14	1.06	0.11
C/BC/B-4-1200	14	1.08	0.14	1.08	0.15
C/BC/B-5-1200	14	1.09	0.15	1.10	0.18
All FE (each grade)		1.13	0.17	1.12	0.17
Collated Exp	34		1.27	1.29	
All (both grades)	202		mean 1.14	COV 0.18	

6.4 Reliability analysis

In order to assess the reliability of the proposed design method, a statistical analysis was conducted. Initially, a comparison between the predicted capacities (R_{pred}) against the experimental/FE obtained capacities ($R_{exp/FE}$) is presented in Figure 18. As can be seen, the points are generally below the diagonal unity line, showing predictions on the safe side. Following the provisions of annex D EN 1990 (CEN, 2002), the proposed method was then statistically validated. Table 8 summarises the following key statistical parameters: the number of tests and FE simulations (n), the design (ultimate limit state), the fractile factor ($k_{d,n}$), the average ratio of test (or FE) to model resistance based on a least-squares fit to all the data ($\bar{b}$), the CoV of the tests and FE simulations relative to the resistance model (V_δ), the combined CoV incorporating both model and basic variable uncertainties (V_r) and the partial safety factor for member resistance (γ_{M1}). Based on the reliability analysis considerations provided in Su et al. (2017), the material over-strength of HSS was taken equal to 1.10 with a CoV of 0.050, while the CoV of geometric properties was assumed to be equal to 0.02 (Gkantou et al., 2017b). The variation between the experimental and the numerical results was also considered (V_{FEM}=0.1). Performing a first-order reliability method in accordance with the Eurocode target reliability requirements, the partial factors were evaluated. The derived partial safety factors for all assessed methods are presented in Table 8. The highest safety factor is required for the AA method, whiles for the proposed method γ_{M1} was found to be γ_{M1}= 1.04, which is lower than the partial safety factor currently employed to Eurocode 9 which is equal to 1.10.

Table 8: Reliability analysis parameters

Design methods	**n**	**$k_{d,n}$**	**$\bar{b}$**	**V_b**	**V_r**	**γ_{m1}**
EC9 - Method A	202	3.139	1.031	0.057	0.100	1.01
EC9 - Method B	202	3.139	1.052	0.066	0.105	1.02
DSM	202	3.139	1.211	0.146	0.168	1.13
DSM - proposal	202	3.139	1.044	0.084	0.117	1.04
AA	202	3.139	1.180	0.177	0.195	1.19

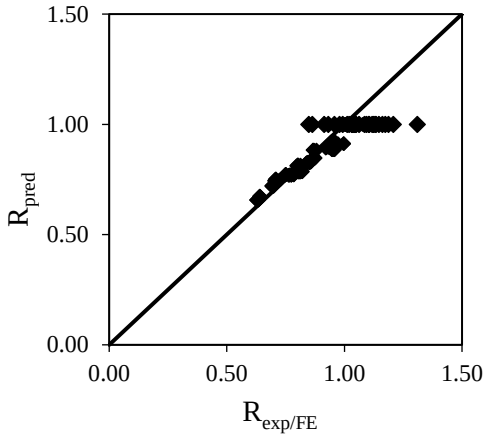

(a) Eurocode – Method A (γ_{m1} = 1.01)

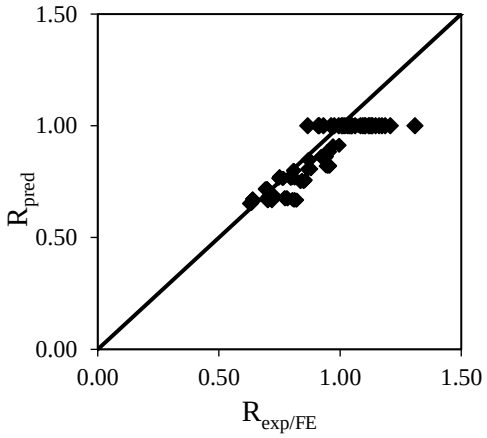

(b) Eurocode – Method B (γ_{m1} = 1.02)

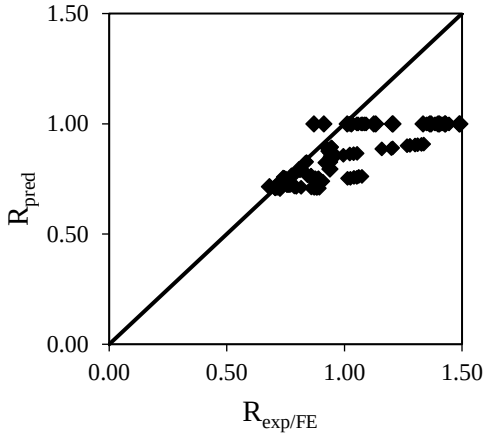

(c) DSM (γ_{m1} = 1.13)

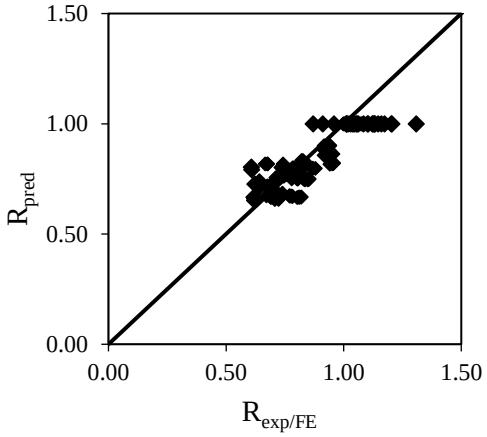

(d) DSM proposed (γ_{m1} = 1.04)

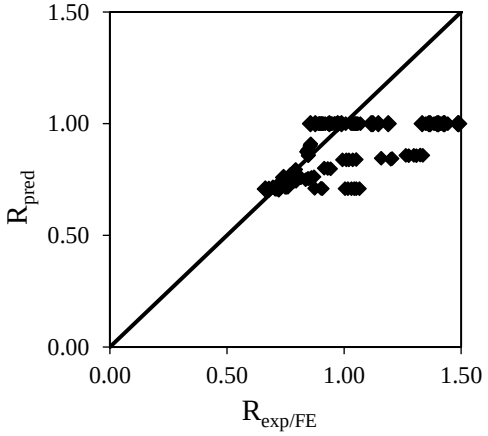

AA (γ_{m1} = 1.19)

471

472 Figure 18: Comparison between predicted (R_{pred}) and experimental/numerical capacities
473 ($R_{exp/FE}$) for the assessed methods.

7. Conclusions

This paper presented a comparative assessment of design models available for the design of aluminium alloy CHS members with stocky sections subjected to compression and bending. In order to ensure an adequate validation of the FE model, a total of 34 experiments (20 beams, 8 columns and 6 beam-columns) based on three research papers were used. A comprehensive numerical investigation on members subjected to a range of eccentric loading conditions was presented. The results were presented graphically on the M-N interaction curves, whilst the predicted capacity ratios were also plotted against the angle θ and tabulated. Subsequently, the numerical results combined with the test data were used for the assessment of the European design provisions, the Direct Strength Method and the Aluminium Design Manual. The main observations and conclusions are listed below.

(1) A mesh convergence and geometric imperfection sensitivity study were performed, demonstrating that D/20 was the optimum mesh size for all members and that the imperfection amplitude t/10 + L/1000 obtained the best agreement between the experimental and numerical results.

(2) The highest accuracy was achieved by the European design provisions, and in particular for the case of $\psi_c = 1.3\chi$ for Class 1 and Class 2 cross-sections. This method resulted in a mean value for R equal to 1.01.

(3) The most conservative predictions were given by the DSM method, resulting in R with mean values of 1.16 and 1.15, based on the FE data of 6082-T6 and 6061-T6, respectively.

(4) Taking into account the DSM buckling strength and the plastic moment resistance, a new interaction curve is proposed that can accurately predict the behaviour of members made of stocky circular hollow sections and subjected to combined compression and bending (mean R value of 1.04).

(5) The design method with the lowest design consistency was AA, resulting in COV equal to 18%.

(6) The design proposal presented herein is based on the results of CHS members made from 6082-T6 and 6061-T6. It is expected that any aluminium alloy material with similar material properties, in terms of overall response, hardening and ductility parameters, could be applicable to this proposal. However, further research on different structural aluminium alloys would be recommended to support this assumption.

References

- Ali, S.B., Kamaris, G.S., Gkantou, M. and Kansara, K.D. (2022) Concrete-filled and bare 6082-T6 aluminium alloy tubes under in-plane bending: Experiments, finite element analysis and design recommendations. Thin-Walled Structures, 172, p.108907.
- Aluminum design manual (AA) (2000). Washington, DC: The Aluminum Association; 2000.
- Aluminum design manual (AA) (2015). Aluminum Design Manual. The Aluminum Association, Washington, D.C., USA.
- AS/NZS (1997) Aluminum structures Part 1: limit state design, Australian/New Zealand standard AS/NZS 1664.1. Sydney, Australia: Standards Australia; 1997.
- Bock, M., Theofanous, M., Dirar, S. and Lipitkas, N. (2021) Aluminium SHS and RHS subjected to biaxial bending: Experimental testing, modelling and design recommendations. Engineering Structures, 227, p.111468.
- Buchanan, C., Gardner, L. and Liew, A., 2016. The continuous strength method for the design of circular hollow sections. Journal of Constructional Steel Research, 118, pp.207-216.
- Castaldo, P., Nastri, E. and Piluso, V. (2017) FEM simulations and rotation capacity evaluation for RHS temper T4 aluminium alloy beams. Composites Part B: Engineering, 115, pp.124-137.
- CEN (European Committee for Standardization) (2002) EN 1990: Eurocode–basis of structural design. CEN, Brussels, Belgium
- Dassault Systèmes Simulia Corp. Abaqus/CAE (2021).
- Eurocode 9 (EC9) (2000) Design of aluminum structures—Part 1-1: general rules—general rules and rules for buildings, DD ENV 1999-1- 1:2000, Final draft Oct 2000. European Committee for Standardization; 2000.
- Eurocode 9 (EC9) (2007) Design of Aluminium Structures - Part 1-1: General Structural Rules. European Committee for Standardization. EN 1999-1-1, CEN. Brussels, Belgium.
- Feng, R. and Liu, J. (2019) Numerical investigation and design of perforated aluminium alloy SHS and RHS columns. Engineering Structures, 199, p.109591.
- Feng, R., Chen, Z., Shen, C., Roy, K., Chen, B. and Lim, J. (2020) Flexural capacity of perforated aluminium CHS tubes–An experimental study. Structures, 25.
- Feng, R., Mou, X., Chen, A., and Ma, Y. (2016) Tests of aluminium alloy CHS columns with circular openings. Thin-Walled Structures, 109, 113-131.

- Georgantzia, E., Ali, S.B., Gkantou, M., Kamaris, G.S., Kansara, K.D. and Atherton, W. (2021a) Flexural buckling performance of concrete-filled aluminium alloy tubular columns. Engineering Structures, 242, p.112546.
- Georgantzia, E., Gkantou, M., & Kamaris, G. S. (2021b) Aluminium alloys as structural material: A review of research. Engineering Structures, 227, 111372.
- Georgantzia, E., Gkantou, M. and Kamaris, G.S. (2023). Aluminium alloy channel columns: Testing, numerical modelling and design. Thin-Walled Structures, 182, p.110242.
- Gkantou, M., Theofanous, M., Wang, J., Baniotopoulos, C., & Gardner, L. (2017a) Behaviour and design of high-strength steel cross-sections under combined loading. Proceedings of the Institution of Civil Engineers-Structures and Buildings, 170(11), 841-854.
- Gkantou, M., Theofanous, M., Antoniou, N. and Baniotopoulos, C. (2017b) Compressive behaviour of high-strength steel cross-sections. Proceedings of the Institution of Civil Engineers-Structures and Buildings, 170(11), pp.813-824.
- Hu, Y., Rong, B., Zhang, R., Zhang, Y., & Zhang, S. (2021) Study of buckling behavior for 7A04-T6 aluminum alloy rectangular hollow columns. Thin-Walled Structures, 169, 108410.
- Li, B., Wang, Y., Wang, Z., Zhi, X., Zhang, Y. and Ouyang, Y. (2022a). 7A04-T6 high-strength aluminium alloy SHS and RHS beams under pure bending—Testing, modelling and design recommendations. Thin-Walled Structures, 177, p.109400.
- Li, B., Wang, Y., Zhang, Y., Meng, X., Yuan, H. and Zhi, X., 2022(b). Flexural buckling of extruded high-strength aluminium alloy SHS columns. Thin-Walled Structures, 179, p.109717.
- Li, B., Wang, Y., Zhang, Y., Zhi, X., & Lin, S. (2022c) Flexural buckling of high-strength aluminium alloy CHS columns. In Structures (Vol. 43, pp. 223-233). Elsevier.
- Li, B., Wang, Y., Zhi, X., Zhang, Y. and Baniotopoulos, C.C. (2022d) Testing, modelling and design of 7A04-T6 high-strength aluminium alloy RHS columns under axial compression. Journal of Building Engineering, 57, p.104910.
- Mazzolani, F.M. Aluminum Alloy Structures, second ed., E & FN Spon, London (1995)
- Nastri, E., Piluso, V. and Pisapia, A. (2022) Experimental tests on SHS aluminium beams under non-uniform bending. Engineering Structures, 267, p.114649.

- Ramberg, W. and Osgood, W.R., 1943. Description of stress-strain curves by three parameters (No. NACA-TN-902).
- Rong, B., Guo, Y. and Li, Z. (2022a). Study on the stability behavior of 7A04-T6 aluminum alloy square and rectangular hollow section columns under axial compression. Journal of Building Engineering, 45, p.103652.
- Rong, B., Zhang, Y., Zhang, S. and Li, Z. (2022b). Experiment and numerical investigation on the buckling behavior of 7A04-T6 aluminum alloy columns under eccentric load. Journal of Building Engineering, 45, p.103625.
- Schafer, B. W. (2008). The direct strength method of cold-formed steel member design. Journal of constructional steel research, 64(7-8), 766-778.
- Su, M.N., Young, B. and Gardner, L. (2016) Flexural response of aluminium alloy SHS and RHS with internal stiffeners. Engineering Structures, 121, pp.170-180.
- Su, M.N., Young, B. and Gardner, L., 2017. Classification of aluminium alloy cross-sections. Engineering Structures, 141, pp.29-40.
- Wang, J., Afshan, S., Gkantou, M., Theofanous, M., Baniotopoulos, C., & Gardner, L. (2016). Flexural behaviour of hot-finished high strength steel square and rectangular hollow sections. Journal of Constructional Steel Research, 121, 97-109.
- Wang, Y., Fan, F. and Lin, S. (2015) Experimental investigation on the stability of aluminium alloy 6082 circular tubes in axial compression. Thin-Walled Structures, 89.
- Wang, Y., Fan, F. and Lin, S. (2015) Experimental investigation on the stability of aluminium alloy 6082 circular tubes in axial compression. Thin-Walled Structures, 89.
- Wang, Y.Q., Wang, Z.X., Yin, F.X., Yang, L., Shi, Y.J. and Yin, J. (2016) Experimental study and finite element analysis on the local buckling behavior of aluminium alloy beams under concentrated loads. Thin-walled structures, 105, pp.44-56.
- Wang, Y., Lin, S., Feng, F., Zhai, X. and Qian, H. (2016) Numerical simulation of aluminum alloy 6082-T6 columns failing by overall buckling. Advances in Structural Engineering, 19(10).
- Yun, X., Wang, Z. and Gardner, L. (2021) Full-range stress–strain curves for aluminum alloys. Journal of Structural Engineering, 147(6), p.04021060.
- Zhao, Y. and Zhai, X. (2020). Bending strength and design methods of the 6082-T6 aluminum alloy beams with circular hollow sections. Structures, 26, pp. 870-887. Elsevier.

- Zhao, Y., Zhai, X. and Wang, J. (2019a) Buckling behaviors and ultimate strengths of 6082-T6 aluminum alloy columns under eccentric compression–Part I: Experiments and finite element modeling. Thin-Walled Structures, 143, p.106207.
- Zhao, Y., Zhai, X. and Wang, J. (2019b) /. Thin-Walled Structures, 143, p.106208.
- Zhi, X., Wang, Y., Li, B., Zhang, Y. and Ouyang, Y. (2022) Axial compression behaviour of 7A04-T6 high-strength aluminium alloy SHS and RHS stub columns. Thin-Walled Structures, 180, p.109816.
- Zhu, J and Young, B. (2009). Design of aluminum alloy flexural members using direct strength method. Journal of structural engineering, 135(5), 558-566.
- Zhu, J. and Young, B. (2006b). Aluminum alloy tubular columns—Part II: Parametric study and design using direct strength method. Thin-Walled Structures, 44(9), 969-985.
- Zhu, J. and Young, B. (2006) Aluminum alloy circular hollow section beam-columns. Thin-Walled Structures, 44(2)
- Zhu, J. and Young, B. (2008) Numerical investigation and design of aluminum alloy circular hollow section columns. Thin-Walled Structures, 46(12).